

A comprehensive literatures update of clinical researches of superparamagnetic resonance iron oxide nanoparticles for magnetic resonance imaging

Yi Xiáng J. Wáng¹, Jean-Marc Idée²

¹Department of Imaging and Interventional Radiology, Faculty of Medicine, The Chinese University of Hong Kong, Prince of Wales Hospital, Sha Tin, New Territories, Hong Kong SAR, China; ²Guerbet, Research and Innovation Division, Roissy-Charles de Gaulle, France

Correspondence to: Yi Xiáng J. Wáng, PhD, MMed, Dipl.-Rad. Department of Imaging and Interventional Radiology, Faculty of Medicine, The Chinese University of Hong Kong, Prince of Wales Hospital, Sha Tin, New Territories, Hong Kong SAR, China. Email: yixiang_wang@cuhk.edu.hk.

Abstract: This paper aims to update the clinical researches using superparamagnetic iron oxide (SPIO) nanoparticles as magnetic resonance imaging (MRI) contrast agent published during the past five years. PubMed database was used for literature search, and the search terms were (SPIO OR superparamagnetic iron oxide OR Resovist OR Ferumoxytol OR Ferumoxtran-10) AND (MRI OR magnetic resonance imaging). The literature search results show clinical research on SPIO remains robust, particularly fuelled by the approval of ferumoxytol for intravenously administration. SPIOs have been tested on MR angiography, sentinel lymph node detection, lymph node metastasis evaluation; inflammation evaluation; blood volume measurement; as well as liver imaging. Two experimental SPIOs with unique potentials are also discussed in this review. A curcumin-conjugated SPIO can penetrate brain blood barrier (BBB) and bind to amyloid plaques in Alzheimer's disease transgenic mice brain, and thereafter detectable by MRI. Another SPIO was fabricated with a core of Fe₃O₄ nanoparticle and a shell coating of concentrated hydrophilic polymer brushes and are almost not taken by peripheral macrophages as well as by mononuclear phagocytes and reticuloendothelial system (RES) due to the suppression of non-specific protein binding caused by their stealthy “brush-afforded” structure. This SPIO may offer potentials for the applications such as drug targeting and tissue or organ imaging other than liver and lymph nodes.

Keywords: Superparamagnetic resonance iron oxide; superparamagnetic iron oxide (SPIO); contrast agent; magnetic resonance imaging (MRI); MR angiography, sentinel lymph node; lymph node metastasis

Submitted Feb 10, 2017. Accepted for publication Feb 20, 2017.

doi: 10.21037/qims.2017.02.09

View this article at: <http://dx.doi.org/10.21037/qims.2017.02.09>

Introduction

Superparamagnetic iron oxide (SPIO) nanoparticles have received much attention in bioscience research since the first report in the 1980s. Biocompatible SPIO nanoparticles with proper surface architecture attracted extensive research efforts for both cellular imaging and drug delivery applications in the past decade. Key features of SPIOs include their ability to exhibit magnetization only in an applied magnetic field; their ability to form stable colloidal suspensions which is crucial for in vivo biomedical

applications (*Figures 1,2*); faster T₂/T₂* relaxation and such can be utilized as magnetic resonance imaging (MRI) contrast agent.

Desirable SPIO features also include the ability to control their composition, size, shape, and surface chemistry. Extensive work has been done on synthesis and surface modification of SPIOs to yield desirable properties (1,2). Traditionally, SPIO usually refers to superparamagnetic iron oxide SPIO nanoparticles with a hydrodynamic size of about 100 nm, which are retained by the reticuloendothelial

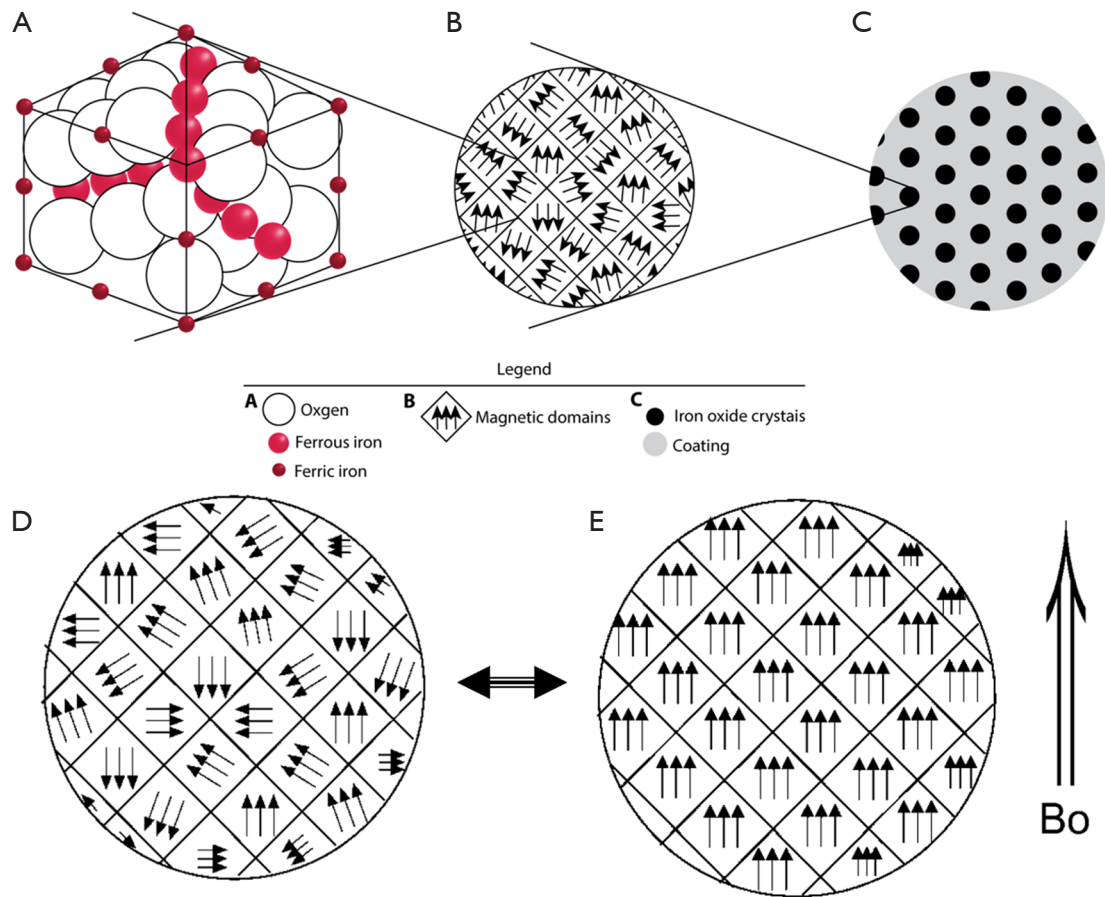


Figure 1 Schematic representation of (A) spinal crystal structure for SPIO domain, (B) SPIO crystal with multiple magnetic domains of random orientation and (C) complete SPIO contrast agent particle, with multiple SPIO crystals and coating materials. (D) SPIO crystal in the absence of an external magnetic field, the orientation of the magnetic domains is random. (E) An external magnetic field (B_0) causes the magnetic domains of the SPIO crystal to reorient according to B_0 , which is reversible after the B_0 is removed. SPIO, superparamagnetic iron oxide.

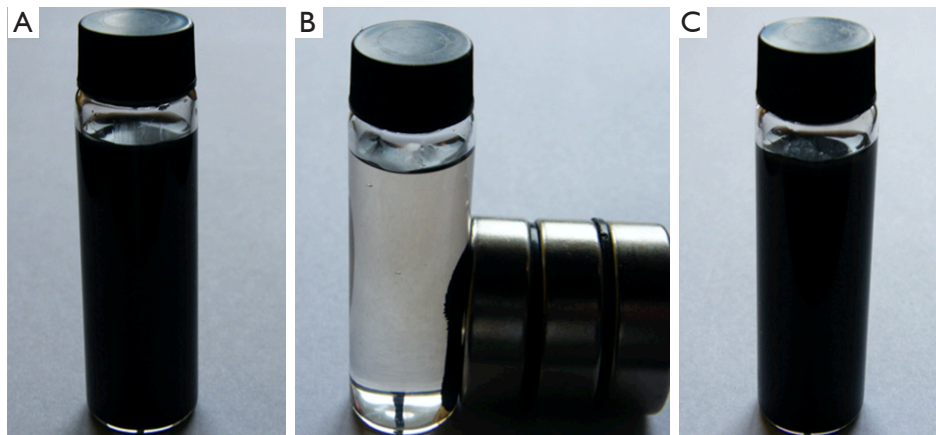


Figure 2 Superparamagnetic property of SPIO. (A) Homogeneous SPIO particle homogeneous suspension in a vial; (B) SPIO particles are attracted by a magnet placed close to one side wall of a vial; (C) after the remove of the external magnet, the SPIO particles can be homogeneously dispersed again, with no residual magnetic property. SPIO, superparamagnetic iron oxide.

system (RES), while USPIO (ultra-small SPIO) which tend to escape RES system initially and are trapped in “deep” macrophagic compartments. We try to use the generic names as much as possible; since true SPIO, i.e., Ferumoxides, is rarely used these days, SPIO may refer to USPIO in this review (the same as in some literatures), readers may need to check with original studies in cases of clarification is required.

Tumor specific imaging via ‘*molecular MRI*’ that uses specific SPIO has been studied in the literature in the last 20 years. However, none of the reported molecular MRI is currently used for routine clinical diagnostic evaluation, nor are any in clinical development. This raises questions as to whether SPIO-enhanced molecular MRI is sensitive and specific enough for use in clinical practice (3-6). In the review article on Iron oxide-loaded nanotheranostics, Schleich *et al.* (6) asked, why do so many papers describe nanomedicines while only a few nanomedicines are commercialized? Dassler and colleagues at the CT and MR Contrast Media Research division of Bayer Pharma AG (Berlin, Germany) investigated the minimum requirements for obtaining sensitive molecular MRI for use in tumor evaluations under optimal conditions (7). The well-vascularized F9 teratocarcinoma tumor model, which exhibits high levels of the highly accessible target CD105 (endoglin, a glycoprotein which is involved in the angiogenesis process), was used to demonstrate the accumulation and visualization of target-specific SPIOs by MRI. SPIOs were optimized by: (I) proton relaxivity was increased; (II) a coating material was used for optimal loading density of the α CD105 antibody; and (III) binding activity to the target CD105 was increased. Binding activity and specificity were confirmed *in vitro*. The transverse relaxation rate $R2^*$ was quantified by 3.0-T MRI in the tumors, kidneys, and muscles before and up to 60 minutes after injection in 11 mice. High-relaxivity α CD105-polyacrylic acid-SPIOs with strong binding activity accumulated specifically in tumors (and kidneys). In contrast to the successful use of MRI in all examined kidneys, only 6 of 11 tumors showed a clear signal when compared with the control even though optimal conditions were used. Dassler and colleagues concluded that the accumulation of CD105-specific SPIOs in F9 mouse teratomas was robust. However, visualization of the specifically accumulated SPIOs by MRI was not reliable because of its limited signal detection sensitivity. They further postulate that molecular MRI by targeted SPIOs is not suitable for clinical tumor imaging using currently available clinical 3.0-T MRI technology (7).

Due to this reason and other obstacles discussed and published (3-6,8-12), this review avoids discuss ‘*molecular MRI*’ of SPIO using such approaches for tumor specific imaging.

For this study, according to the suggestion of *Quant Imaging Med Surg* for literature review (13), PubMed (www.ncbi.nlm.nih.gov/pubmed/) database was used and the search terms were (SPIO OR superparamagnetic iron oxide OR Resovist OR Ferumoxytol OR Ferumoxtran-10) AND (MRI OR magnetic resonance imaging); and the search was updated on 5th Feb 2017. Focus was on clinical studies involving human subjects and data were published during the past 5 years [2012–2016]. Two novel SPIOs having particular interesting characteristics with potential future clinical translation are also discussed in this review. The primary aim of this review is to provide an overview for non-clinical readers, particularly for biomaterial researchers who like to research on SPIO. For in-depth discussion of clinical topics, readers should refer to the original publications. As only PubMed database was used, the literature search might not be comprehensive (13). However, it is believed that a broad picture can still be drawn covering important clinical research activities for SPIO.

Under normal circumstances, intravenously injected SPIO with hydrodynamic size of about 100 nm is sequestered by Kupffer cells and other cells from the RES, bone marrow, spleen, and thereafter metabolized and regulated by normal physiological iron homeostatic mechanisms. This SPIO sequestration may protect liver cells from apoptosis because only free iron oxides have been proven to be toxic. Nevertheless, repeated SPIO dosing in short intervals is not a desirable option for imaging and drug delivery because it could lead to surpassed transferrin iron-binding capacity and to high free iron concentrations. For a translational approach, toxicity assessments should be performed on case by case basis. A number of clinical safety issues of clinical approved SPIO have been described, thought the incidence is overall uncommon (14-19). Importantly, SPIO is not indicated in pregnant women. For example, ferumoxytol (marketed North America as Feraheme[®] by AMAG Pharmaceuticals for the treatment of iron deficit anemia) is classified as Pregnancy Category C [as are gadolinium-based contrast agents (GBCA)] by the United States Food and Drug Administration (20). Small animal trials have linked ferumoxytol administration (at very high doses) to birth defects, including soft-tissue malformations and decreased fetal weights (20). To date, human data are unavailable; however, the existing animal

data suggest that ferumoxytol should not be administered during pregnancy. By comparison, iodinated contrast agents are classified as Pregnancy Category B and have a more favorable safety profile in pregnancy (21). In 2015, FDA issued a Drug Safety Communication after a search of the FDA pharmacovigilance database identified 79 cases of hypersensitivity reactions associated with ferumoxytol. Eighteen of these 79 cases were fatal. Consequently, FDA issued a Boxed Warning, FDA's strongest type of warning (22). This impacted the availability of ferumoxytol in Europe. SPIO may also affect the function of labeled cells, such as Chang *et al.* (23) reported amine-surface-modified SPIO nanoparticles interfere with differentiation of human mesenchymal stem cells; Cromer-Berman *et al.* (24) reported motility of neural stem cells is reduced after SPIO-labeling, which is mitigated after exocytosis. However, clinical safety is not the main focus of this review.

Available SPIO/USPIO agents

While many research groups developed various their own SPIO materials, this review is focused on the agents developed by pharmaceutical companies and those have underwent some stages of clinical trials. Factors of SPIO's size, coating materials, relaxivity, etc. all lend the SPIOs have different *in vitro* and *in vivo* properties. A number of SPIO agents have underwent various stages of clinical trials for MRI, and some of them have been approved by regulatory bodies (25,26). Feridex[®] (Ferumoxides, Feridex[®] IV, Berlex Laboratories, Endorem[®], France) and Resovist[®] (Ferucarbotran, Resovist[®], Bayer Healthcare, Germany) were primarily designed for liver imaging, and received regulatory approval in USA and Europe respectively, as well as in Japan. Feridex[®] cannot be administered as an intravenous bolus as it could be associated severe back pain, while Resovist[®] can be administered by fast bolus injection. Due to the lack of users, Feridex[®] (Endorem[®]) been withdrawn from the market, and Resovist[®] is current available in only limited countries, such as Japan (Resovist[®]; FUJIFILM RI Farma Co., Ltd., Kyobashi, Tokyo, Japan). NC100150 (Clariscan[®], Nycomed, Norway) and (VSOP C184, Ferropharm, Germany) have been designed and clinically tested for MR angiography and blood pool imaging (27,28), but did not achieve regulatory approval. Silica coated SPIO Ferumoxsil (Lumirem[®], or GastroMARK[®]) was approved as a useful oral contrast agent for darkening of bowel loops, but was also taken off the market due to lack of users. There is a recent report

that oral SPIO contrast agent before Magnetic Resonance Cholangiopancreatography improves the visualization of extrahepatic biliary ducts in patients with ascites which is helpful during the liver surgery (particularly for liver transplantation) (29).

Ferumoxytol (Feraheme[®], AMAG Pharmaceuticals, Cambridge, MA; note the marketing authorization for Rienso[®], i.e., ferumoxytol in Europe, has been withdrawn at the request of Takeda Inc., ferumoxytol is currently not available in Europe) has been approved for the treatment of iron deficiency in adult chronic kidney disease patients (30). It is comprised of iron oxide particles surrounded by a carbohydrate coat, has a colloidal particle size of 30 nm and a molecular weight of 750 kD. Ferumoxytol injection is a sterile liquid with a neutral pH, formulated with mannitol for isotonicity. Ferumoxytol parenteral iron therapy can be used to treat iron deficiency anemia in patients with chronic kidney disease and other chronic diseases and represents an attractive alternative to oral iron therapy with more effective results based on a recent systematic review (31). Ferumoxytol demonstrates a $r1$ relaxivity of $15 \text{ mmol}^{-1}\text{s}^{-1}$, and a $r2$ relaxivity of $89 \text{ mmol}^{-1}\text{s}^{-1}$. Thus, ferumoxytol causes enhancement on T1-weighted images, but also causes susceptibility effects on T2-weighted images. It can be administered via bolus intravenous injection, and initially behaves as a blood pool agent. Due to its relatively large molecular size, there is little leakage of the agent into the extravascular/interstitial compartment and little renal clearance. However, this compound is not approved for imaging purposes yet.

It has been pointed out that ferumoxytol treatment for iron deficiency anemia can obscure enhancement from GBCA for days or weeks following administration (32,33). MRI has demonstrated measurable amounts of residual iron in the liver for months following ferumoxytol administration in healthy subjects, with clearance times ranging from 3 to more than 11 months. Diagnosticicians should be aware of the potential effects on MRI examinations after ferumoxytol administration, as they can confound the interpretation of these examinations. Ferumoxytol-enhanced T2*-weighted MRI also shows normal adrenal loses signal (34). The bone marrow uptake of ferumoxytol and T2* enhancement may also help to distinguishing normal or hypercellular marrow from neoplasms (35).

Ferumoxtran-10, (formerly Sinerem[®], Guerbet, Roissy, France; and Combidex[®], AMAG Pharmaceuticals, Cambridge, MA, USA) was primarily designed for lymph node MRI. Despite initial very promising data (36), the

pivotal study failed to demonstrate a statistically significant benefit for sensitivity and failed to confirm non-inferiority with regard to specificity (37). Therefore their clinical development was halted. However, some authors argue that to interpret SPIO enhanced lymph node MRI, high level of experience is required. Experienced interpreters may offer much better sensitivity and specificity for SPIO-enhanced MRI of lymph node metastasis (38). Ferumoxtran-10 is now under development by a spin-off company, SPL Medical BV (<https://www.splmedical.com/>), of Nijmegen University, the Netherlands.

Sienna plus[®] is a dark brown aqueous suspension of organically coated SPIO particles with a particle size of 59 nm (*Figure 3*). It is injected subcutaneously where the natural physical action of the lymphatic system filters out the particles, enabling sentinel nodes to be located using the Sentimag[®] (*Figure 3*). Sienna+[®] is a Class IIa device, CE-approved for marketing and sales in Europe, and ARTG (Australian Register of Therapeutic Goods) listed for Australasia. In USA, Sienna+[®] is limited to investigational use only under an FDA-approved Investigational Device Exemption (IDE). Sienna plus[®] (Sienna+[®], information available from www.endomag.com/sienna) was provided by Endomag, which was founded in 2007 as a spin-out from the University College London and the University of Houston. According to Endomagnetics Ltd, key features and benefits of Sienna plus[®] include: (I) particle size optimised for filtration and retention by sentinel lymph nodes; (II) localisation can start after only 20 minutes following injection, but injection can be up to 7 days in advance; (III) natural dark brown colour eliminates the need for separate (carbon or blue) dye injections; (IV) long shelf life; (V) calibrated for use with handheld probe Sentimag[®].

To summary, currently ferumoxytol and Resovist[®] are currently available for clinical use intravenously, though most of the recent MRI literatures deal with investigational (off-label) applications of these two agents, rather than the clinically indicated (approved) applications. In the following sections various investigational applications involving SPIO are discussed.

USPIO MR angiography

Since ferumoxytol is an iron-based agent with no potential for causing nephrogenic systemic fibrosis, it may be useful as an alternative to linear GBCAs in patients with compromised renal function. Nephrogenic system fibrosis has been described and found to be associated with or

caused by linear gadolinium contrast agent administration in renal-impaired patients (Chronic Kidney Disease stages 4 and 5) (38-42). Nephrogenic systemic fibrosis is a potentially morbid and deadly disease characterized by soft-tissue contractures and occasionally cardiopulmonary compromise. With more judicious gadolinium contrast agent dosing, careful attention to patient risk factors, and use of gadolinium contrast agents with relatively favorable safety profiles (i.e., macrocyclic Gd chelates), the incidence of nephrogenic system fibrosis appears to have fallen substantially. Nonetheless, awareness of this disease has prompted active interest in non- GBCAs.

Ferumoxytol causes enhancement on T1-weighted images, and has a long intravascular half-life on the order of 14–15 hours, making it a potentially useful agent for vascular and perfusion-weighted MRI. As a blood pool contrast agent, ferumoxytol provides a much longer temporal window for data acquisition than extracellular agents, allowing imaging to be performed repeatedly beginning as early as the arterial phase and continuing into later phases. This could be of use in imaging of smaller arteries, where extended imaging periods could be leveraged to obtain high-resolution imaging with high signal-to-noise ratio, in applications where venous enhancement can be tolerated (43-49) (*Figure 4*). Compared to those with kidney transplants, many patients with severe renal insufficiency are dependent on hemodialysis via a peripheral arteriovenous fistula. MR angiography with ferumoxytol can evaluate arteriovenous fistula patency, while MR angiography using the linear GBCAs gadodiamide, gadoversetamide and gadopentetate is contraindicated in this patient population (49).

Detecting aortic endoleaks after endoluminal stent graft repair can be performed with contrast-enhanced CT angiography or with contrast-enhanced MR angiography. However, like extracellular GBCAs, iodinated contrast agents used in CT are rapidly excreted, and intravascular signal degrades quickly with time. This creates a clinical dilemma, since low-flow endoleaks may accumulate contrast media slowly, and the optimal imaging time to detect these lesions is undetermined. Ferumoxytol has been shown to display small and slow endoleaks, even hours after injection, due to its long blood pool half-life. Ersoy *et al.* (50) found that ferumoxytol was useful for detecting subtle, intermittent, or gradual extravasation of blood from the intravascular space (i.e., endoleaks) after endoluminal stent-graft repair of infrarenal aortic aneurysms. In Ersoy *et al.*'s study, ferumoxytol-enhanced MR angiography delineated the location and volume of endoleak as well as the feeding

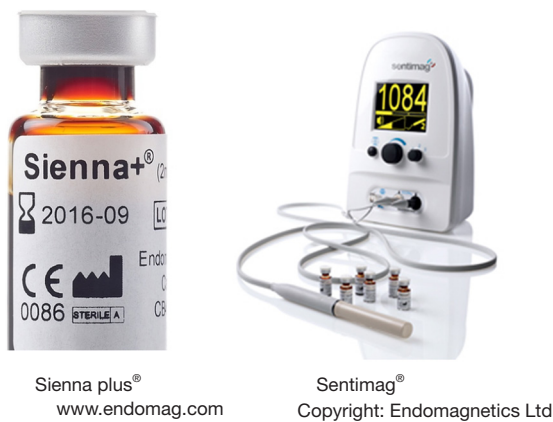


Figure 3 A picture of Sienna plus® and its detector Sentimag® (Copyright: Endomagetics Ltd).

vessels, information that is extremely important for patient management (50). Repeated MR angiography after 24 hours was also useful for calculating the endoleak rate.

The effect of ferumoxytol on blood pressure has been noted. Ning *et al.* (48) reported the use of ferumoxytol in 86 pediatric patients and young adults. The mean \pm standard deviation pre and post-contrast systolic blood pressures were 101 ± 18 and 95 ± 20 , respectively. There was a statistically significant difference between pre-systolic blood pressures and post-systolic blood pressures ($P=0.003$). The pre-contrast diastolic blood pressures and the post-contrast diastolic blood pressure were 60 ± 14 and 51 ± 17 , respectively. There was a statistically significant difference between pre-diastolic blood pressure and post-diastolic blood pressure ($P<0.001$). Therefore, in their sample, there was on average a small but clinically insignificant drop in systolic blood pressures and post-diastolic blood pressure ferumoxytol injection. The authors recommended that large, randomized, controlled trials are needed to establish optimal dosing, imaging procedures, and safety monitoring.

Sentinel lymph node detection with SPIO (interstitial MR lymphography)

Surgeons earlier had advocated wide excision and elective lymph node dissection to control lymphatic permeation of metastases. Arguments in favor of elective lymph node dissection include better survival of patients with clinically negative, histologically positive lymph nodes relative to patients with clinically apparent metastases to the regional nodes. An argument against elective lymph node dissection

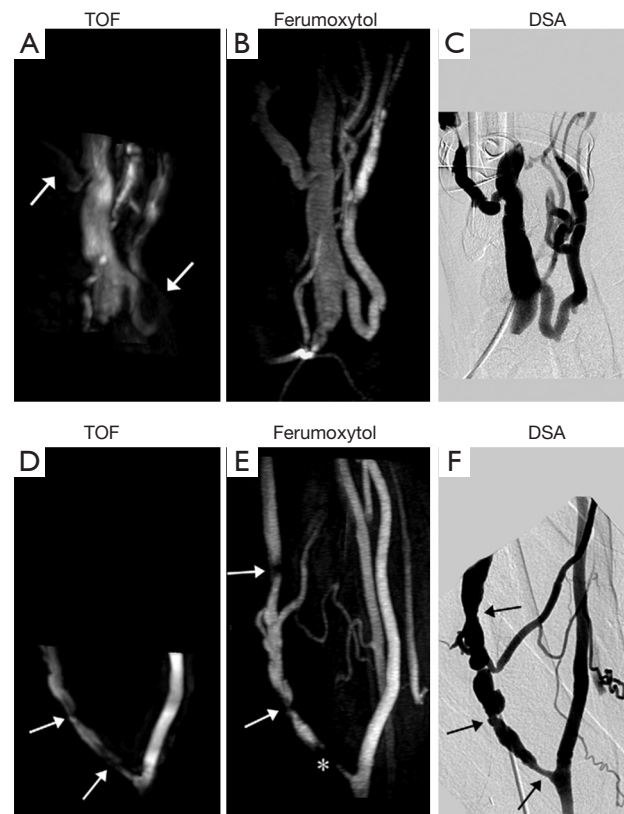


Figure 4 Comparison of TOF MR angiography, ferumoxytol enhanced MR angiography, and X-ray digital DSA. (A-C) MIP images of radiocephalic wrist fistula (1 month after surgery). TOF MIP image shows low signal intensity in the arterial inflow and side branch on the venous outflow (arrows); these regions are clearly depicted on the ferumoxytol-enhanced MR angiography MIP image. Note that the TOF coverage of the vascular anatomy is only half the coverage of the ferumoxytol-enhanced MR angiogram. Absence of stenosis was confirmed by using DSA; (D-F) MIP images of brachiocephalic elbow fistula (8 months after surgery). TOF MIP image illustrates two stenotic regions (arrows). Ferumoxytol-enhanced MR angiography MIP image shows three stenotic regions, two distal to the anastomosis (arrows) and one proximate that appears occluded (*). Note the improved volume coverage of the ferumoxytol-enhanced MR angiography that enables detection of stenosis missed at TOF imaging. All three stenotic regions were confirmed on DSA image [Reprinted with permission (49)]. MIP, maximum intensity projection; TOF, time of flight; DSA, digital subtraction angiography.

is that patients are sometimes unnecessarily subjected to a morbid surgical procedure. Procedure cost, morbidity, and the low yield of tumorous nodes have led to a reduction in

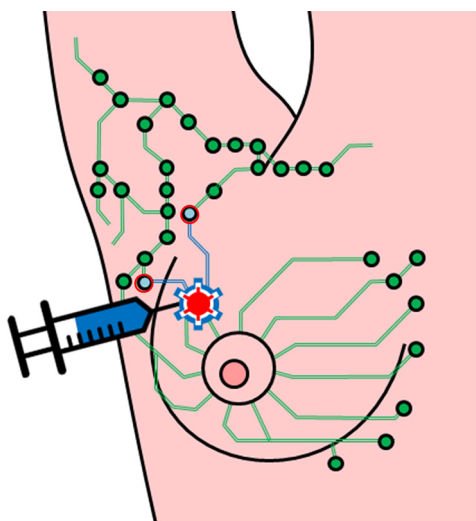


Figure 5 Schematic representation of the sentinel lymph node localization procedure, showing the peritumoral injection site, and tracer travelling to two sentinel lymph nodes which can be biopsied and further evaluated for histopathologically.

the routine use of elective lymph node dissection, although tumor status of the nodes is important for determining prognosis and the need for adjuvant therapy (51). Detection of occult regional node metastases has been improved by intraoperative lymphatic mapping and sentinel lymphadenectomy. This technique maps the direct lymphatic path from the primary to the regional nodes and permits selective excision of the first (“sentinel”) lymph node(s) (Figure 4). Because the sentinel lymph node is the likely site of early metastatic tumor, *focused pathologic examination* permits the accurate staging of regional nodes (for details, see reference 51). Sentinel lymph node biopsy has become the standard of care that has replaced axillary lymph node dissection as a less invasive method for axillary staging in breast cancer patients with clinically negative nodes (51). Sentinel node biopsy decreases the risk of morbidity in terms of lymph edema, neuropathies, seroma, wound infection, reduced shoulder motility, and chronic pain. Additionally, neoadjuvant treatment for breast cancer has further widened the indications of sentinel node biopsy.

Identification of the sentinel lymph node is based on the use of a radioactive tracer, most often in combination with a carbon or blue dye injected interstitially, either close to the breast areola or around the tumor (51). The combination of these two methods has been established as the gold

standard for the detection of the sentinel lymph node. However, the use of an isotope demands a nuclear medicine setup. The short half-life (6 h) of Technetium^{99m} limits its usefulness and also confers hazards to the patient and staff. Moreover, complicated legislation and restrictions regulate the handling and disposal of radioactive material. The carbon dye can be allergenic with reported incidence varies between 0.07% and 2.7% (52), and has been associated with rare cases of serious events. These facts stress the need for nonradioactive and non-allergenic tracers with an ability to detect the sentinel lymph node comparable to the traditional methods.

SPIO-enhanced techniques are being evaluated for detecting metastases in sentinel nodes. SPIO can be one of the agents which have been approved clinically (such as Resovist[®]), or newly designed SPIO (such as Sienna plus[®]). SPIO enhanced sentinel lymph nodes are detected by MRI (53), or by a hand-hold sterile probe which seek sentinel nodes for further histopathological evaluation (Figure 5).

The method of a combination of CT lymphography and SPIO-enhanced sentinel node MRI is explained in details by Motomura *et al.* (53) (Figure 6). After local anesthesia, iodinated contrast agent was injected intradermally into the skin overlying the breast tumor and into the subareolar skin. A CT scan was performed after massaging the iodinated contrast agent injection site. SPIO (a 40- μ L aliquot of Resovist, containing 1.115 mg iron, diluted in 20 mL normal saline, as per Motomura *et al.*, (53) was administered locally, similar to the administration of dye and radioisotope during sentinel node detection. The injection sites of SPIO were gently massaged for 1 min. At 18 to 24 h after the administration of SPIO, the T1-, T2-, and T2*-weighted sequences used for interpretation of the lymph node status are repeated (36). Nodes are evaluated on pre-SPIO and post-SPIO images. A node was considered nonmetastatic if it showed homogenous low signal intensity and metastatic if the entire node or a focal area did not show low signal intensity on post-SPIO MRI compared with the signal intensity on pre-SPIO images (36) (Figure 7).

In the series of 102 patients with breast cancer and clinically negative nodes, Motomura *et al.* (53) reported the mean number of sentinel nodes identified by CT lymphography was 1.1 (range, 1–3). The sensitivity, specificity, and accuracy of 1.5T MRI for the diagnosis of sentinel node metastases were 84.0%, 90.9%, and 89.2%, respectively. In 4 of 10 patients with micro-metastases, metastases were not detected, but all 15 patients with

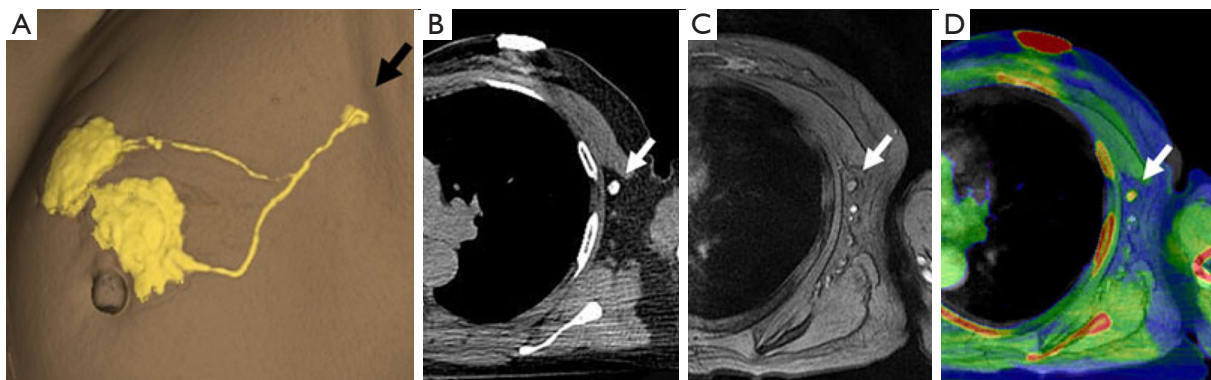


Figure 6 Three-dimensional CT lymphography reconstructed from the first post-iodinated contrast images (A). Iodinated contrast agent is injected intradermally into the skin overlying the breast tumor and the subareolar skin. Lymphatic vessels are drained into a single axillary sentinel node (arrow, A). Images of CT lymphography (B) and T2*-weighted axial MR images (C) at the same level are compared to specify the node (arrow) on T2*-weighted axial MRI corresponding to the sentinel node (arrow) identified by CT lymphography. If necessary, images of CT lymphography and T2*-weighted axial MR images can be merged on a workstation (D) [Reprinted with permission (53)].

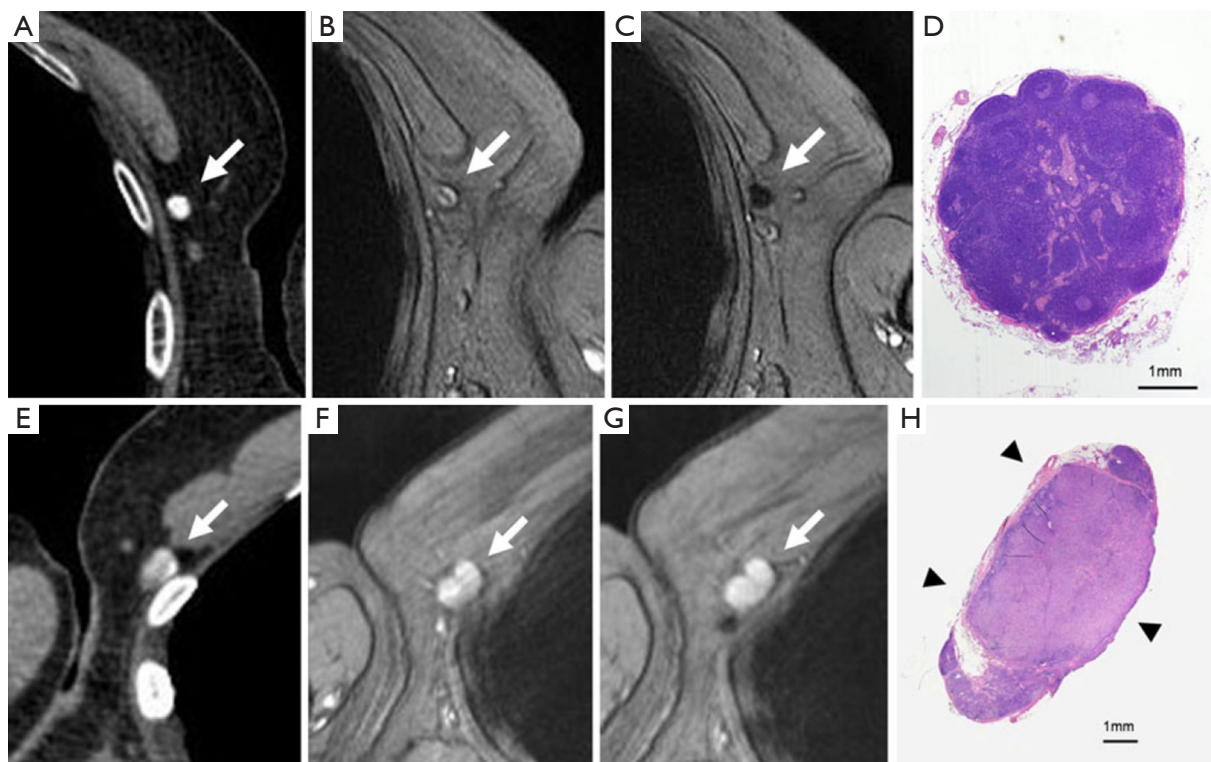


Figure 7 Resovist enhanced MRI demonstrates metastasis negative and positive lymph nodes. (A) CT lymphography demonstrates a sentinel node (arrow); (B) the corresponding node is identified on pre-SPIO-contrast T2*-weighted axial MRI (arrow), showing high signal intensity; (C) after administration of SPIO, the node shows strong SPIO enhancement and was diagnosed as benign (arrow); (D) histologic findings confirmed it as benign; (E) CT lymphography demonstrates a sentinel node (arrow); (F) the corresponding node is identified on pre-SPIO-contrast T2*-weighted axial MRI (arrow), showing high signal; (G) after administration of SPIO, the node shows no SPIO enhancement and is diagnosed as malignant (arrow); (H) histologic findings confirmed it as malignant. This node is almost entirely replaced by metastatic tissue (arrowheads) [Reprinted with permission (53)]. SPIO, superparamagnetic iron oxide; MRI, magnetic resonance imaging.

macro-metastases were successfully identified. Motomura *et al.* (53,54) further suggested excessive dosage or a high concentration of SPIO may conceal small metastatic foci, resulting in low signal intensity of the whole sentinel node. Micro-metastases of 2 mm or smaller would be difficult to detect accurately. With initial 100-fold and 200-fold dilution of SPIO, even macro-metastases were missed in some cases. Then Motomura *et al.* decided to use 500-fold dilution. Motomura *et al.* (53) commented that further study is needed to explore the best timing and concentration of SPIO to improve the accuracy of this technique, such as fat-suppressed images, higher field magnet (as opposed to the 1.5T system used in the study of reference 53), and a special radiofrequency coil may improve accuracy.

Further reports have been published, such as reference (55-59). Mizokami *et al.* (59) reported a study on sentinel node detection by interstitial MR lymphography with Resovist[®] in tongue cancer patients who also underwent lymphoscintigraphy. The sentinel nodes were clearly visualized in the 10 min interstitial MR lymphography images and were completely concordant with those visualized by ^(99m)Tc-radiocolloid lymphoscintigraphy and a gamma probe in all cases. Iron incorporation into the sentinel lymph nodes was confirmed by pathological examination. MR sentinel lymphography with SPIO as a tracer offer better imaging quality, in contrast to the poor spatial resolution of scintigraphy. This may be a promising perspective in cases where preoperative localization will still be needed such as in melanomas of the trunk and head and neck, and recurrent breast cancer, where the lymphatic drainage is sometimes distorted (60,61). Data from a meta-analysis indicate that USPIO have sensitivity and specificity for the detection of axillary involvement of 98% and 96% respectively (62). Meng *et al.* (63) suggested that if MRI could accurately diagnose axillary lymph node metastases in early stage breast cancer, the most cost-effective strategy was to replace sentinel lymph node biopsy with axillary MRI.

Detection of sentinel lymph nodes with SPIO can be done by a simple hand-held probe (*Figure 3*) (64-67). A number of studies with the combination of Sienna plus[®] and SentiMag[®] (Endomagentics Ltd) have been reported. After injection in the breast, Sienna plus[®] drains through the lymphatics and accumulates in the sentinel lymph node. The handheld probe SentiMag[®] is used to identify the sentinel lymph node, in the same way as the gamma probe is used for detection of isotope-containing nodes. The solution is dark brown, and the nodes are often colored,

which can help the surgeon identify the sentinel lymph node visually as well. In the Nordic SentiMag trial (68), two mL of Sienna plus[®] diluted with 3 mL saline was injected subareolarly either shortly before or after induction of anesthesia. The injection site was massaged for 5 min, and the operation was not to start until at least 20 min had elapsed. During operation, SentiMag[®] was first used to detect magnetic uptake. A short incision was made in the axilla over the area with the greatest uptake, and the sentinel node was sought for primarily using the SentiMag probe. The brownish coloring of the sentinel lymph node when SPIO is used can be an aid intraoperatively to detect sentinel lymph node for histopathology (68). Researches till now have shown non-inferiority for SPIO over conventional techniques for sentinel lymph node detection (isotopes ± carbon or blue dye) (69-75). This new method does not have the disadvantages of the standard technique and is promising as a safe and effective alternative in the absence of nuclear medicine facilities. However, without MRI, this technique does not assess the internal structure of lymph node.

It should be noted that after SPIO such as Sienna plus[®] administration, both MRI and hand-held probe (such as SentiMag[®]) can be used in the same session to detect SPIO enhanced lymph nodes. In a small cohort of 11 patients, Pouw *et al.* (76) reported interstitially administered SPIO can be used both for pre-operative imaging and intra-operative sentinel lymph node biopsy, with equal performance to imaging and localization with radioisotopes. They described that it is a feasible technique for pre-operative localization of sentinel lymph nodes and, in combination with intra-operative use of a handheld magnetometer, provides an entirely radioisotope-free technique for sentinel lymph nodes biopsy. Carbon coated SPIO nanoparticles, which suit both for sentinel lymph node evaluation as well as can function as dark carbon dye, has also been reported, though it did not move to clinical trial yet (77).

In a 2011 meta-analysis paper Harnan *et al.* (62) commented that SPIO-enhanced MRI showed a trend towards higher sensitivity and specificity and may make a useful addition to the current diagnostic pathway. However, current estimates of sensitivity and specificity do not support replacement of sentinel lymph node biopsy for identifying axillary node metastases in breast cancer patients with MRI technology. Additional larger studies with standardised methods and standardised criteria for classifying a node as positive are needed (62). In a 2014

review paper Ahmed *et al.* (78) suggested that modern imaging and biopsy greatly help the axillary staging of breast cancer. Selective therapeutic axillary surgery should be based upon preoperative imaging findings. Sentinel lymph node biopsy, which requires histopathology evaluation, may become redundant with SPIO-enhanced MRI. Overall, additional well-designed and statistically-powered studies are needed to better evaluate the value of this technique

Intravenously administered USPIO enhanced MRI for lymph node metastasis evaluation

Tumor staging, choice of therapy, and patient prognosis are highly dependent on the spread of a primary malignant tumor to regional and distant lymph nodes. Currently, surgical procedures and imaging techniques with inherent weaknesses are used to obtain this crucial information of nodal involvement for staging purposes. An intraoperative exploration used to sample lymph nodes at the time of primary tumor resection is performed, particularly in malignancies in which imaging has a low accuracy. This approach of surgical staging with lymphadenectomy and histopathologic evaluation of the lymph nodes is considered the gold standard in patients with various malignancies such as prostate cancer. However, it is invasive, confined to the surgical field for nodal sampling which may lead to sampling errors, and only yields limited accuracy. For cross-sectional imaging, the primary criterion for assessing lymph nodes by CT and MRI is nodal size. However, lymph node size is not a reliable parameter for the evaluation of metastatic involvement. The size criterion frequently overlooks metastases particularly if only microscopic or partial metastases of the lymph node are involved. Specificity may be reduced by benign inflammatory or infectious lymph node enlargement, which leads to the incorrect characterization of a benign lymph node as malignant.

The standard practice for intravenously administered SPIO enhanced MRI for lymph node metastasis evaluation is to perform SPIO enhanced imaging with two MRI scans performed 24 to 36 hours apart (36). It has also been suggested that there is no significant difference in diagnostic precision between paired MRI and post-contrast MRI alone for an experienced reviewer (79). In this case, contrast material could be injected in the patient at a site remote from the MR suite, and the patient could return the next day for a single MRI examination. However, two scans of pre-contrast and post-contrast still remain the standard practice till now. In a lymph node with preserved

architecture and function, macrophages take up a substantial amount of ferumoxtran-10. This physiological uptake of ferumoxtran-10 results in a marked reduction in signal intensity of the lymph nodes. Infiltration of lymph nodes with malignant cells replaces macrophages and alters nodal architecture; hence the lymph nodes lack uptake of ferumoxtran-10 and either retain their high signal intensity after contrast administration or display a heterogeneous signal intensity if only partial or micro-metastases are involved (8,80) (Figures 7,8). For lymph nodes between 5 and 10 mm, sensitivity was 96% and specificity was 99%, and for lymph nodes smaller than 5 mm, sensitivity and specificity were reduced to 41% and 98%, respectively (81).

Lahaye *et al.* (82) found that the most accurate and practical predictive criterion for assessing malignant lymph nodes on ferumoxtran-10 enhanced MR images in patients with primary rectal cancer is the estimation of percentage of white region (high signal intensity) within the lymph node. An estimated area of white region within the node that was larger than 30% was highly predictive for an involved node, with a sensitivity of 93% and a specificity of 96%. The larger the area of the white region, the more likely that the node is malignant. A high signal intensity or white region in the lymph node is caused by no or very little uptake of SPIO in that part of the lymph node. Because of the lack of macrophages, benign conditions such as focal nodal fibrosis, granulomatous disease, or a fatty hilum can be depicted as a white region as well, thus mimicking malignant nodes. These white regions, however, are usually 30% or less of the total nodal area (82).

Fortuin *et al.* (83) reported that the mean diameter of the detected suspicious lymph nodes on ferumoxtran-10 enhanced MRI was significantly smaller than those detected by PET/CT, being 4.9 and 8.4 mm, respectively. In 61% patients, suspicious lymph nodes were found outside the clinical target volume with ferumoxtran-10 enhanced MRI and in 31% patients with PET/CT. The authors concluded that ferumoxtran-10 enhanced MRI detects lymph nodes suspicious for metastasis, irrespective of the existing size and shape criteria for CT and conventional MRI. Therefore ferumoxtran-10 enhanced MRI and PET/CT can help to individualize treatment selection and enable image-guided radiotherapy for patients with prostate cancer lymph node metastases.

However, MRI with current technology has a limited spatial resolution. False-negative results might be due to microscopic metastases that are below the detection threshold of current MRI scanners. Lymph node MRI false-

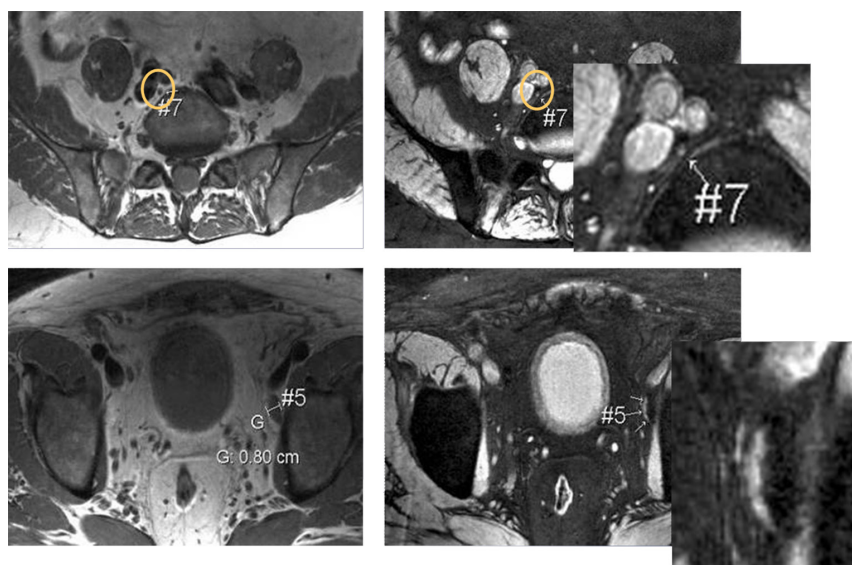


Figure 8 This figure shows that how small lymph nodes supposed to be benign due to their size can be malignant. Images on the left hand are pre-contrast images, while the post-ferumoxtran-10 images on the right show hypersignal intensity small lymph nodes, which is a sign of malignancies. MRI at 3T allows depiction of these small lesions with high spatial resolution [Reprinted with permission (1)]. MRI, magnetic resonance imaging.

positive results can be due to reactive hyperplasia (focal nodal fibrosis, granulomatous disease), inflammatory swollen lymph nodes, post treatment changes, localized nodal lipomatosis or a prominent fatty hilum, and insufficient dosage of ferumoxtran-10 (80,84).

Though the European Medicines Agency did not approved ferumoxtran-10-enhanced MRI for the detection of metastases in lymph nodes due to the unfavorable pivot study result (37), the debate on its value is still on-going and being further investigated. Investigator initiated studies have been continuing (85,86). Triantafyllou *et al.* (85) reported the diagnostic accuracy of Resovist[®]-enhanced MRI for the detection of metastases in normal sized lymph nodes using extended pelvic lymph node dissection and histopathology as the reference standard. A total of 2,993 lymph nodes were examined histopathologically. Fifty-four metastatic nodes were found in 20/75 patients (26.7%). The first reading had a sensitivity of 55.0%, specificity of 85.5%, and diagnostic accuracy of 77.3% on a per patient level. The second reading had a mean sensitivity of 58.3%, specificity of 83.0%, and diagnostic accuracy of 76.4% on a per patient level. The majority of missed metastases were smaller than 5 mm in short axis diameter. Fortuin *et al.* (87) pointed that the diagnostic performance of that study can be improved by using T2* based sequence, and also

interpreter's experience is of crucial importance, which may also impact the impact of these agents on daily practice (and their market access), since the learning curve may be long. It is expected experienced readers and standardized evaluation protocol would have led to a better outcome (88).

Ferumoxylol, like other SPIO agents, is not cleared by glomerular filtration but by macrophages in the RES, and this feature could also serve to help detect pathology in the RES where normal uptake is not observed, such as in the diagnosis of metastatic lymphadenopathy. Recently McDermott *et al.* (89) evaluated ferumoxylol enhanced MRI in identifying malignant nodal involvement in patients with pancreatic ductal adenocarcinoma. Lymph nodes that lacked contrast uptake were deemed malignant, and those that demonstrated homogeneous uptake were deemed benign. They reported sensitivity and specificity was 76.5% and 98.4% at a nodal level and 83.3% and 80% at a patient level. On the other hand, conventional cross-sectional imaging (CT, MRI, and PET/CT) has been found to have a sensitivity of 0% to 42% in nodal staging of pancreatic cancer. McDermott *et al.* further commented that in their patient cohort using a 1-cm short-axis diameter threshold, or even the more conservative 8-mm threshold, none of the malignant nodes would have been correctly characterized. With the administration of ferumoxylol, the sensitivity

increased from 0% to 76.5%. Ferumoxytol enhanced MRI correctly identified five of six patients with pathology-proven lymph node involvement. It failed to identify nodal involvement in one patient in which there was a very small metastatic focus in one lymph node. Alternatively, in the only case where ferumoxytol enhanced MRI falsely diagnosed lymph node involvement on pathologic review, it was nodular extension of the primary tumor rather than an involved lymph node. Turkbey *et al.* (90) sought to determine the optimal dose of ferumoxytol for performing MR lymph node imaging at 3T in patients with prostate cancer. They suggested that the dose level of 7.5 mg Fe/kg ferumoxytol was safe and effective, which can be the starting point for future phase II studies regarding the efficacy of ferumoxytol for MR lymphadenopathy. Atri *et al.* (91) evaluated whether ferumoxtran-10 improves accuracy of MRI to detect lymph node metastasis in advanced cervical cancer. They reported that ferumoxtran-10 increased MRI sensitivity to detect lymph node metastasis in advanced cervical cancer; however the diagnostic specificity remained a concern.

USPIO enhanced MRI for inflammation process evaluation

Following intravenous injection, USPIO is incorporated into macrophages via endocytosis. The uptake of USPIOs by phagocytic monocytes and macrophages provides an *in vivo* tool by which MRI can be used to monitor the involvement of macrophages in inflammatory processes, such as multiple sclerosis (MS), stroke, brain tumors, and vulnerable plaque in carotid artery (1,92-99).

Macrophages are important components of inflammatory processes in MS, closely linked to axonal loss, and can now be observed *in vivo* using SPIO (such as SHU-555C, Bayer Healthcare, Germany; and ferumoxtran-10). Tourdias *et al.* (94) reported comparing MRI features of MS lesions after the administration of a GBCA and ferumoxtran-10 among different clinical phenotypes of MS and over time. SPIO enhanced MRI was obtained 24-48 after ferumoxtran-10 administration. With 56 lesions were considered active owing to contrast enhancement at baseline; 37 lesions (66%) in 10 patients enhanced with GBCA. The use of SPIO helped detect 19 additional lesions (34%), and two additional patients were classified as having active disease. Thus, the use of both agents enabled detection of 51% (19 of 37 lesions) more lesions than with GBCA alone. Ferumoxtran-10 enhancement, in the form of ring-like

patterns, could also be observed on T1-weighted images in patients with progressive MS, enabling the detection of five lesions in addition to the five detected with GBCA in this phenotype. Lesions that enhanced with both contrast agents at baseline were larger and were more likely to persistently enhance at 6-month follow-up compared with those that enhanced only with gadolinium or USPIO. Therefore the combination of GBCA and ferumoxtran-10 in patients with MS can help identify additional active lesions (Figure 9). Lesions that enhance with both agents may exhibit a more aggressive evolution than those that enhance with only one contrast agent. Crimi *et al.* (95) reported that patients can be classified according to the nature of inflammatory lesions patterns, and this characterization can infer new prospective from the earliest imaging signs of MS. Maarouf *et al.* (96) sought to determine the prevalence and the impact on tissue injury of macrophage infiltration in patients after the first clinical event of MS. Their results suggested that SPIO (SHU-555C)-positive lesions reflecting infiltration of macrophages. This infiltration was associated with local higher loss of tissue structure and persistent local loss of tissue structure. Farrell *et al.* (97) reported that ferumoxytol or ferumoxtran-10-enhanced brain MRI can be useful in the diagnosis of central nerve system inflammatory disorders (demyelination or inflammation) and lymphoma (lymphoma or lymphoproliferative disorder), and is also useful for patients with renal compromise at risk of nephrogenic systemic fibrosis who are unable to receive GBCA.

Atherosclerosis is fundamentally an inflammatory disease involving macrophages and T cells. Pathological studies of carotid atherosclerosis implicate macrophages in increasing the risk of fibrous cap rupture and they occur with greater frequency in plaques in symptomatic patients. There is a clear clinical necessity for an inflammatory marker capable of identifying high-risk atherosclerotic plaque. Several earlier clinical studies have shown that ferumoxtran-10 targets macrophages located in atherosclerotic aorta and pelvic arteries or in stenotic carotid arteries (98-100). Ferumoxtran-10 induces MRI-detectable signal loss in macrophage-rich plaques. The earlier Atorvastatin Therapy: Effects on Reduction of Macrophage Activity (ATHEROMA) study investigated the effects of low- and high-dose atorvastatin on carotid plaque inflammation as determined by ferumoxtran-10 enhanced carotid MRI in 47 patients with carotid artery stenosis >40%. This trial showed the evidence that aggressive lipid-lowering therapy with high-dose of atorvastatin over a 3-month period is associated with significant reduction in SPIO-defined

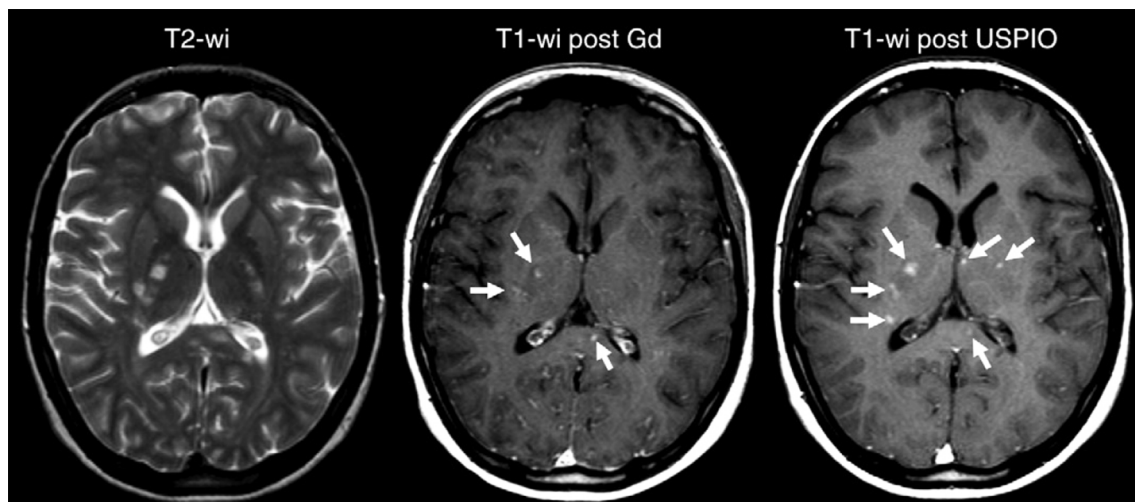


Figure 9 Mismatch between gadolinium- and ferumoxtran-10 enhanced images obtained at baseline in a 23-year-old woman with active relapsing-remitting MS without disease-modifying treatment. Left, axial unenhanced T2-weighted image shows multiple hyperintense lesions. Middle, axial gadolinium-enhanced T1-weighted image shows three enhanced lesions (arrows). Right, axial T1-weighted image obtained 24–48 hours after injection of Ferumoxtran-10 shows the same three lesions along with three additional active lesions that enhanced only with ferumoxtran-10 (arrows) [Reprinted with permission (94)].

carotid plaque inflammatory foci (100). Recent studies of Toll-like receptors offer evidence to support that monocyte activation is associated with larger and symptomatic plaques, again reinforcing the concept of inflammation worsening plaque vulnerability (101,102). USPIOs are thought to enter the inflamed plaque through the dysfunctional endothelium incited by a multitude of insults including cholesterol deposition, free radical damage from superoxides eluted by macrophages, and biomechanical stress. USPIO hypointensity changes can differentiate symptomatic carotid arteries from the contra-lateral asymptomatic side with greater relative signal loss seen in symptomatic patients (99,103). In a recent study, Degnan *et al.* (104) reported an association between SPIO-defined plaque inflammation and developing subsequent vascular events ($P=0.07$). The non-significant (P value =0.07) was considered to be due to the study was inadequately powered (104). Interesting, in hyperlipidemic rabbits, the *in vivo* MRI enhancement was found to be higher with the long half-life agent ferumoxtran-10 as compared to that obtained with ferumoxytol which has shorter half-life, whereas *in vitro* macrophage phagocytosis was greater with ferumoxytol (105).

Intracranial aneurysms and arteriovenous malformations are important indications for clinical MR. It has been shown that the primary pathogenesis in the formation and rupture of intracranial aneurysms is inflammation, and

that endothelial cell injury is associated with macrophage migration into aneurysm walls, smooth muscle cell death, and aneurysm wall weakness (106–108). Thus, the ability of ferumoxytol to depict macrophage distribution makes it a potential tool for intracranial aneurysms imaging. In a small pilot study, Hasan *et al.* (109) showed that intracranial aneurysms with early uptake (within 24 hours) of ferumoxytol were prone to rupture or increase in size, while intracranial aneurysms with late uptake (72 hours) were stable without rupture over a 6-month follow-up period (Figure 10). The same group also performed a study to assess the anti-inflammatory effects of aspirin on intracranial aneurysms. They found that patients treated with aspirin prior to imaging had decreased ferumoxytol uptake in the aneurysm wall compared to patients treated after imaging. This suggested that aspirin caused a decrease in inflammation, an observation which was corroborated on histopathological specimens (110,111). Therefore ferumoxytol-enhanced MRI may provide a noninvasive prognostic assessment of aneurysm stability, risk-stratify lesions in need of early intervention, and may be useful for following the response to medical therapy.

Prediction of abdominal aortic aneurysm (AAA) growth and rupture is challenging and currently relies on serial diameter measurements with ultrasound, and therefore without assessment of the inflammatory status of the aorta wall.

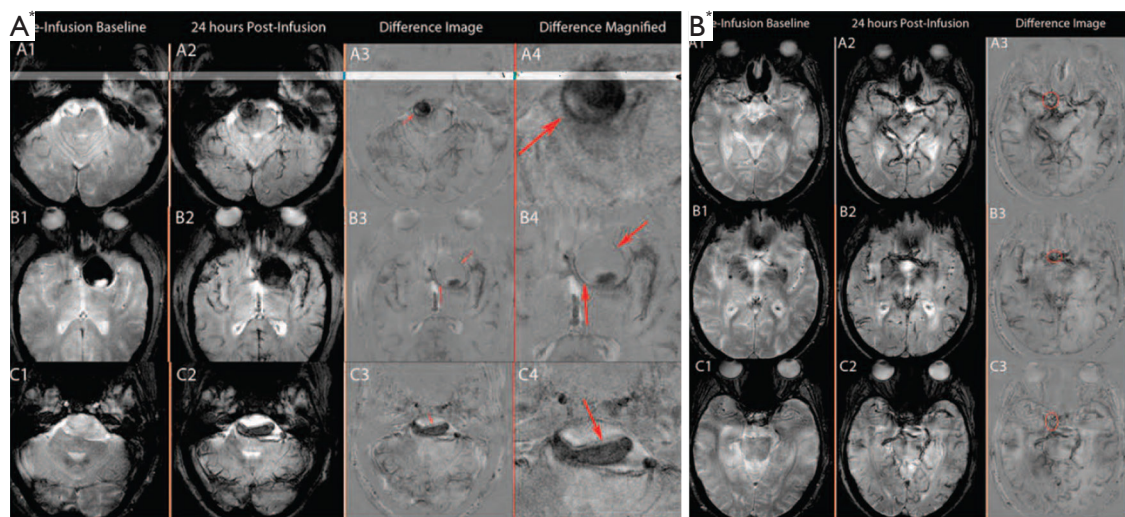


Figure 10 Ferumoxytol-enhanced MRI detects depict macrophage distribution in intracranial aneurysm walls. (A) T2* gradient echo MRI sequence at baseline and 24 hours postinfusion of Ferumoxytol showing early signal changes in the walls of 3 cerebral aneurysms. A1–4, corresponds with a patient a right vertebral artery aneurysm; B1–4, corresponds with a patient with a left supraclinoid internal carotid artery aneurysm; and C1–4, corresponds with a patient with a fusiform vertebrobasilar artery aneurysm). Difference images demonstrate the relative signal loss after ferumoxytol infusion. All 3 aneurysms ruptured within 6 months. (B) T2* gradient echo MRI sequence at baseline and 24 hours postinfusion of Ferumoxytol, and subtraction images showing no early signal changes in 3 aneurysms from three patients (A1–3, right internal carotid artery terminus aneurysm; B1–3, anterior communicating artery aneurysm; and C1–3, right cavernous internal carotid artery aneurysm). None of these aneurysms ruptured during the follow-up period [Reprinted with permission (109)]. MRI, magnetic resonance imaging.

Inflammation is critical in the pathogenesis of AAA disease. Ferumoxytol enhanced MRI has demonstrated promise to identify aneurysm inflammation. McBride *et al.* (112) compared ^{18}F -FDG PET-CT and USPIO-enhanced MRI for assessing tissue inflammation. Fifteen patients with asymptomatic AAA with diameter 46 ± 7 mm underwent PET-CT with ^{18}F -FDG, and T2*-weighted MRI before and 24 hours after administration of SPIO. When all areas of the aneurysm were evaluated, there was a modest correlation between the standardised uptake values (SUVs) on PET-CT and the change in $R2^*$ (i.e., $=1/T2^*$) on USPIO-enhanced MRI. That ^{18}F -FDG PET-CT and USPIO-MRI uptake distinct differences in the pattern and distribution of uptake, suggesting a differential detection of macrophage glycolytic and phagocytic activity respectively. In a systematic review paper Jalalzadeh *et al.* (113) reported that relationship between inflammatory processes (as evaluated by ^{18}F -FDG uptake and USPIO enhanced MRI) and AAA progression remains unclear. To address these issues, the MA (3) RS study (350 patients expected) at Edinburgh and Glasgow is currently on-going and expects to report in 2017 (114) (Figure 11). This is the first study to evaluate the use of

ferumoxytol-enhanced MRI to provide information to aid risk prediction models in patients with AAA.

The inability to visualize the initiation and progression of type-1 diabetes (T1D) noninvasively in humans is a major research challenge. Gaglia *et al.* (115) described a method for imaging the pancreatic inflammation underlying T1D, based on ferumoxytol enhanced MRI. This approach reflects SPIO uptake by macrophages in the inflamed pancreatic lesion. A pilot on patients recently diagnosed with T1D versus healthy controls found that there was a clear difference in whole-pancreas SPIO accumulation in patients and controls, and the patients with T1D exhibited pronounced inter- and intrapancreatic heterogeneity in signal intensity (Figure 12). Malosio *et al.* (116) reported three T1D patients and one nondiabetic patient undergoing autotransplantation following subtotal pancreatectomy received Ferumoxides labelled islets. Their results suggest that MRI monitoring of islet transplantation at early time points could represent a meaningful readout for helping in predicting transplant failure or success; however, its relevance for mid/long-term islet function assessment remains to be confirmed (116).

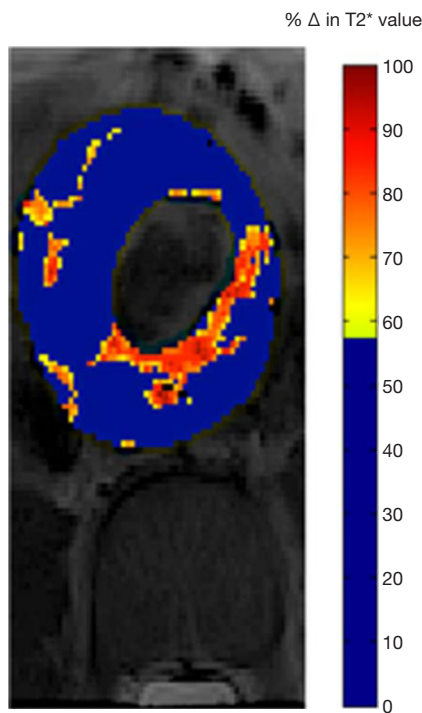


Figure 11 Color map of MRI of an AAA. Red and yellow pixels indicate areas of increased $T2^*$ value, indicative of USPIO uptake [Reprinted with permission (114)]. AAA, abdominal aortic aneurysm; MRI, magnetic resonance imaging.

Inflammation following acute myocardial infarction (MI) has detrimental effects on reperfusion, myocardial remodelling, and ventricular function. Alam *et al.* (117) reported a study of patients with acute ST-segment elevation MI. After intravenous infusion of ferumoxytol (4 mg/kg), in the myocardial infarct $R2^*$ (i.e., $=1/T2^*$) value increased from $41.0 \pm 12.0 \text{ sec}^{-1}$ (baseline) to $155 \pm 45.0 \text{ sec}^{-1}$ ($P < 0.001$) and $124 \pm 35.0 \text{ sec}^{-1}$ ($P < 0.05$) at 24 and 48 hours, respectively. A similar but lower magnitude response was seen in the remote myocardium, where it increased from $39 \pm 3.2 \text{ sec}^{-1}$ (baseline) to $80 \pm 14.9 \text{ sec}^{-1}$ ($P < 0.001$) and $67.0 \pm 15.7 \text{ sec}^{-1}$ ($P < 0.05$) at 24 and 48 hours, respectively. In a case-report study, Yilmaz *et al.* (118) suggested that ferumoxytol enhanced MRI may allow noninvasive detection of the region of acute MI and the peri-infarct zone, and angio-MR analysis showed hypersignal of the aorta up to 48 hours after ferumoxytol administration. Further, Yilmaz *et al.* (119) studied 14 patients who had experienced an acute ST-elevation myocardial infarction. They suggested that SPIO-based

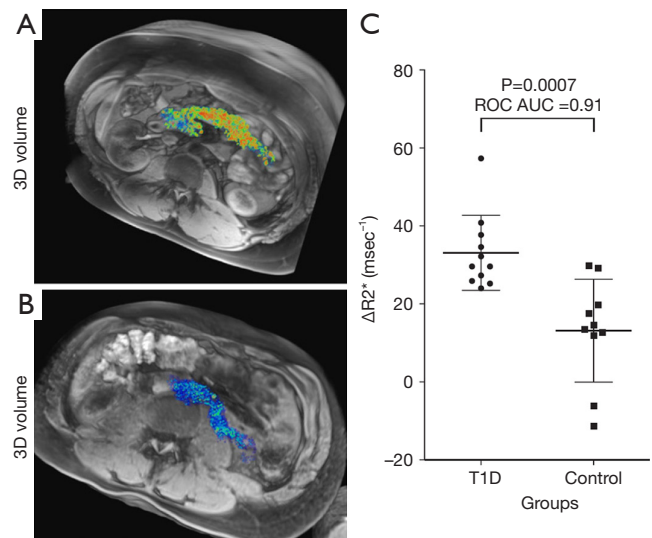


Figure 12 Ferumoxytol enhanced MRI of pancreas shows increased pancreatic SPIO accumulation in patients with type-1 diabetes 3D volume sets of a representative patient with recently diagnosed type-1 diabetes (A) and a normal control subject (B). (C) Comparison of the two cohorts examined by MRI. Plots of global pancreatic $\Delta R2^*$ (i.e., $=1/T2^*$) values are shown for 11 patients with type-1 diabetes and ten normal controls [Reprinted with permission (115), Copyright [2015] National Academy of Sciences of USA]. MRI, magnetic resonance imaging; SPIO, superparamagnetic iron oxide.

contrast agents enable a more detailed characterization of myocardial infarct pathology mainly by detecting infiltrating macrophages.

Labeling peripheral blood mononuclear cells with SPIO (Ferumoxides) has undergone a pilot clinical trial. Richards *et al.* (120) sought to develop a Good Manufacturing Practice-compliant method of labeling competent peripheral blood mononuclear cells with SPIO (ferumoxides), and to evaluate MRI cell tracking in human subjects. Peripheral blood mononuclear cells were labelled with SPIO. Ferumoxides-labelled cells had similar *in vitro* viability, migratory capacity, and pattern of cytokine release to unlabeled cells. Using a phased-dosing study, it was demonstrated that systemic delivery of up to 10^9 SPIO-labelled cells in humans is safe, and cells accumulating in the RES were detectable on clinical MRI. In a healthy volunteer model, a focus of cutaneous inflammation was induced in the thigh by intradermal injection of tuberculin. Intravenously delivered SPIO-labelled cells tracked to the inflamed skin and were detectable with MRI (120).

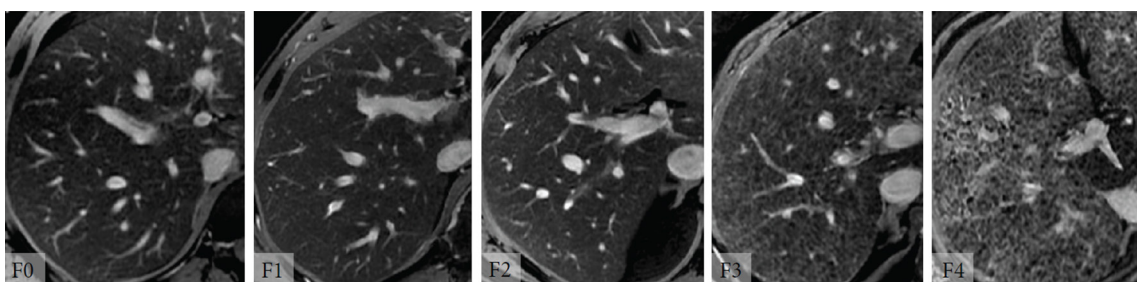


Figure 13 Combined contrast enhanced (ferumoxides and Gd-DTPA) MR images at various stages of fibrosis. Combined contrast enhanced images in adults with chronic hepatitis C virus infection and histologically determined Metavir fibrosis stages F0, F1, F2, F3, and F4. Subjectively, the reticular texture of the liver parenchyma becomes progressively more pronounced with increasing Metavir fibrosis stage [Reprinted with permission (127)].

SPIO enhanced liver MRI

After intravenous administration, SPIO particles of hydrodiameter around 100 nm tended to be filtered from the blood via phagocytosis accomplished by RES system so that uptake is mainly observed in the normal liver and spleen. Phagocytosed SPIO particles in K upffer cells in the liver produce strong T_2/T_2^* relaxation effects in normal hepatic parenchyma. Following the administration of this agent, because of a homogeneous distribution of reticuloendothelial cells in the healthy liver parenchyma, the liver negatively enhances on T2- or T2*-weighted images, resulting in increased conspicuity for pathologic lesions that do not contain reticuloendothelial cells. The degree of SPIO uptake and the consecutive extent of signal intensity drop are used to differentiate and characterize lesions. However, it has been shown that no significant difference in number of K upffer cells between well-differentiated hepatocellular carcinoma (HCC) and the surrounding healthy liver tissue (121), while a difference of K upffer cells distribution between HCC and healthy liver tissue is the basic assumption of SPIO contrast for HCC detection. Some studies show SPIO-enhanced MRI is less efficient than standard Gadolinium-enhanced *dynamic* MRI in the detection and characterization of HCC (122). Currently, hepatocyte-specific contrast agent Gd-EOB-DTPA (Primovist[®], Europe; Eovist[®], USA; Bayer HealthCare) enhanced liver MRI is emerging as the leading method for diagnosis and staging of HCC (123). Moreover, Nishie *et al.* (124) reported that the uptake of Gd-EOB-DTPA in the liver parenchyma decreased as the liver fibrosis progressed, however, no significant correlation was obtained between the parameters on Resovist[®]-enhanced MRI and the histological findings of the liver parenchyma.

Saito *et al.* (125) reported that Gd-EOB-DTPA -enhanced MRI provided more information than Resovist[®]-enhanced MRI in characterizing focal nodular hyperplasia.

Despite the results that Ferumoxides has been withdrawn from the market, research on Ferucarbotran (Resovist[®]) and recently ferumoxytol are still being pursued during the last 5 years, particularly on GBCA and SPIO double contrast, and texture analysis for enhanced MR images for hepatic fibrosis evaluation (126-129) (*Figure 13*). Maurea *et al.* (130) suggested that Ferucarbotran enhanced MRI provides a diagnostic incremental value, particularly to characterize *focal liver lesions* compared to Gd-DTPA enhanced MR; they recommend the use of SPIO when liver lesion characterization is requested and Gd-DTPA enhanced MR images are uncertain (*Figures 14-16*). Liau *et al.* (131) reported that an intravenous infusion of SPIO/USPIO (Feridex) did not affect the IDEAL IQ method of fat quantification. Whether these researches on SPIO will be translated into daily clinical practice remain unknown, due to the complexity of these procedures, and the emerging competing techniques such as Gd-EOB-DTPA-enhanced MRI, improved ultrasound elastography, liver T1rho imaging etc. (132-135).

USPIO enhanced MRI for blood volume measurement

As opposed to the MR angiography where T1 relaxation and enhancement are utilized, USPIO can also be exploited to generate vessel volume using T2* contrast. Varallyay *et al.* (136) and Hanneman *et al.* (137) tested the feasibility of clinical steady-state-cerebral blood volume (CBV) measurement using ferumoxytol (*Figure 17*). The steady-state-CBV maps are feasible using ferumoxytol in a clinical dose of 510 mg, providing higher resolution images with

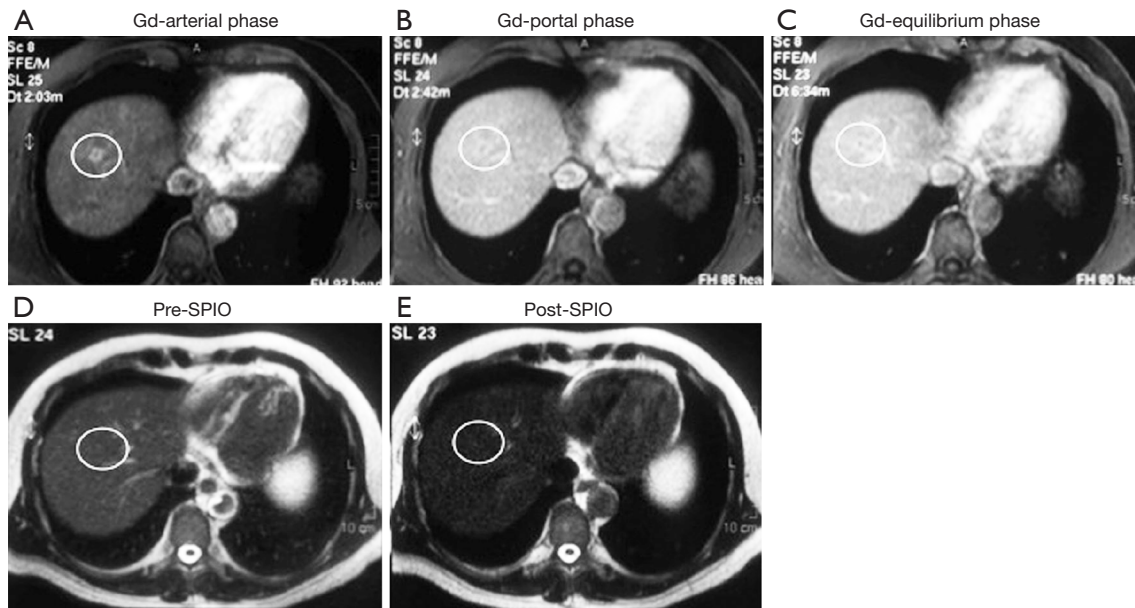


Figure 14 A small (1 cm) capillary hemangioma, proven by biopsy, was located in the segment VIII; dynamic MR images after gadolinium (Gd) administration show focal faint enhancement by the lesion (white circle) only in the arterial phase (A) with no focal abnormality in portal (B) and equilibrium (C) phases (false positive finding); T2 weighted MR images before (D) and after (E) SPIO administration show homogeneous contrast distribution in the liver with diffuse hypointensity and no focal abnormalities (true negative finding) [Reprinted with permission (130)]. SPIO, superparamagnetic iron oxide.

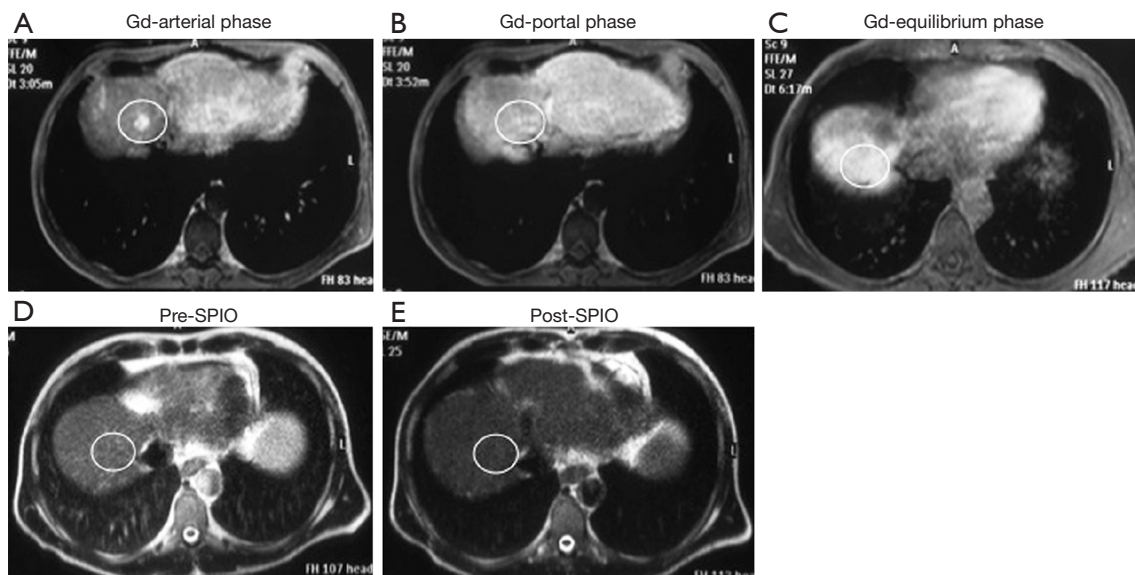


Figure 15 A small (1 cm) dysplastic nodule, proven by biopsy, was located in the segment VIII; dynamic MR images after gadolinium (Gd) administration show focal faint enhancement by the lesion (white circle) only in the arterial phase (A) with no focal abnormality in portal (B) and equilibrium (C) phases (false positive finding); T2 weighted MR images before (D) and after (E) SPIO administration show homogeneous contrast distribution in the liver with diffuse hypointensity and no focal abnormalities (true negative finding) [Reprinted with permission (130)]. SPIO, superparamagnetic iron oxide.

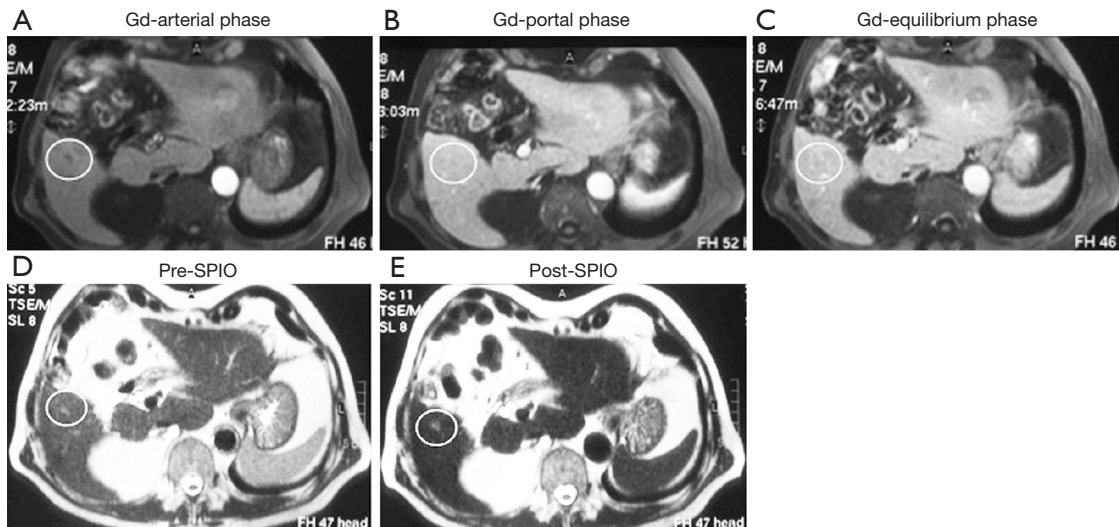


Figure 16 A small (5 mm) hepatocellular carcinoma (HCC), proven by biopsy, was located in the segment VI; dynamic MR images after gadolinium (Gd) administration show no focal abnormalities in the arterial (A), portal (B) and equilibrium (C) phases (false negative finding); T2 weighted MR images before (D) and after (E) SPIO administration show diffuse liver hypointensity and focal faint hyperintensity (white circle) in the VI hepatic segment in the post-contrast MR image (E) (true positive finding) [Reprinted with permission (130)]. HCC, hepatocellular carcinoma; SPIO, superparamagnetic iron oxide.

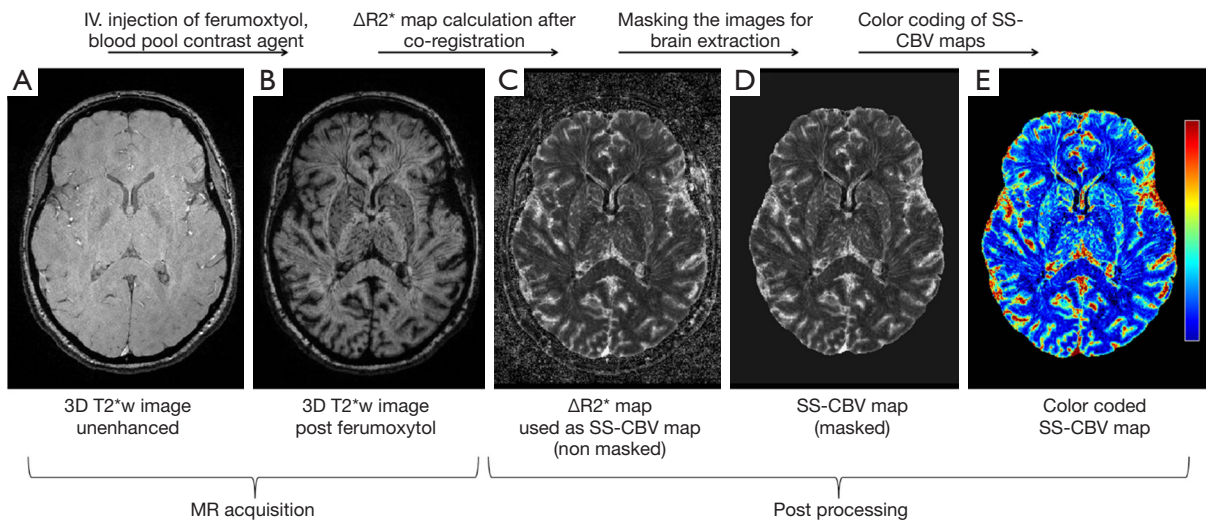


Figure 17 The process of creating SS-cerebral blood volume (CBV) maps. Using pre (A) and post (B) ferumoxytol T2*-weighted (T2*w) images, $\Delta R2^*$ maps (C) can be calculated. $\Delta R2^*$ is assumed to be linearly proportional to contrast agent concentration. Since there is no substantial extravasation of this blood pool agent, $\Delta R2^*$ is derived from the intravascular compartment only and $\Delta R2^*$ maps can be used as SS-CBV maps. To eliminate the noisy background caused by the logarithmic calculation, images were masked (D). The CBV maps are typically displayed with color coding (E) [Reprinted with permission (136)]. SS, steady state; CBV, cerebral blood volume.

comparable relative cerebral blood volume (rCBV) values to the dynamic susceptibility contrast technique obtained with GBCA. They conclude that functional imaging using USPIO will be beneficial in visualizing CNS pathologies with high vascularity that may or may not correspond with blood-brain barrier abnormalities. Fredrickson *et al.* (138) reported the feasibility of acquiring vessel size imaging metrics using ferumoxytol injections in a multicenter Phase I trial of a novel therapy in patients with advanced metastatic disease. Clinical ferumoxytol-based vessel size imaging is feasible with lesions outside of the brain (138).

Radiologic deterioration of brain tumors appears as an enlarged area of enhancement on contrast enhanced T1-weighted MR images. It can reflect either tumor progression or treatment-induced inflammatory change with increased permeability of the blood-brain barrier known as pseudoprogression. Conventional T2-weighted and contrast T1-weighted MRI do not allow differentiation of tumor progression from pseudoprogression. Dynamic susceptibility-weighted contrast-enhanced MRI measurement of rCBV has been used for glioma grading, assessment of prognosis for patients with gliomas, and differentiation of recurrent tumor from radiation necrosis. High rCBV values indicate active neovascularization and a viable tumor. Accurate measurement of tumor rCBV by using standard susceptibility-weighted contrast modeling approaches requires intravascular localization of contrast agent, which is compromised by the leaky blood-brain barrier present in patients with malignant brain tumors, especially after chemoradiotherapy. Rapid extravasation of a low-molecular-weight GBCA can result in underestimation of tumor rCBV. Ferumoxytol is administered as a fast bolus injection, and acts as a blood pool agent and vascular localization is not compromised by the leaky blood-brain barrier. It has the potential to allow measurement of rCBV more reliably than does GBCA. Nasseri *et al.* (139) reported 56 patients with glioblastoma multiforme who demonstrated conventional findings concerning for progression of disease post chemoradiotherapy. Dynamic susceptibility-weighted contrast-perfusion MRI with ferumoxytol was used to distinguish true progression from pseudoprogression using rCBV values with rCBV = 1.75 assigned as the cutoff value. Twenty-seven participants (48.2%) experienced pseudoprogression. Overall survival was significantly longer in participants with pseudoprogression (35.2 months) compared with those who never experienced pseudoprogression (14.3 months). They concluded that ferumoxytol, used as a blood pool

agent, facilitates differentiation between tumor progression and pseudoprogression, appears to be a good prognostic biomarker, and, unlike GBCA, does not require contrast agent leakage correction (139,140) (*Figure 18*).

Bevacizumab (BEV, Avastin, Genentech, Inc.) is an anti-vascular endothelial growth factor (VEGF) A antibody working as an angiogenesis inhibitor that normalizes tumor vasculature, and decreases contrast-enhancing tumor volume and blood volume in lesions both in animal models and clinically. Neovascularization, a distinguishing trait of high-grade glioma, is a target for anti-angiogenic treatment with bevacizumab. Netto *et al.* (141) sought to use ferumoxytol-based dynamic susceptibility contrast MRI to clarify perfusion and relative blood volume (rCBV) changes in glioma treated with Bevacizumab. They found that due to blood volume reduction caused by Avastin treatment, the threshold of rCBV > 1.75, used to differentiate high rCBV from low rCBV after chemoradiotherapy, may be confounded early after Avastin administration and thwart true diagnoses of vascular progression, true response, or treatment related changes.

USPIO/Ferumoxytol enhanced MRI has been explored to increase the sensitivity of fMRI (142-145). Blood oxygen level dependent (BOLD) fMRI is sensitive to concentration of endogenous deoxyhemoglobin, which is paramagnetic. Neuronal activity induces changes in concentration of regional deoxyhemoglobin relative to periods of rest and creates a change in the magnetic susceptibility of blood that can be detected by MRI. Physiological interpretation of the BOLD fMRI signal is complicated by the fact that concentration of deoxyhemoglobin is impacted by both oxygen delivery and consumption, factors which cannot be easily disentangled. BOLD endpoints typically display low signal dynamic range (1–4% relative to baseline BOLD), high variability relative to signal (i.e., low signal-to-noise ratio and low contrast-to-noise ratio) and technical limitations such as scanner instability. SPIO nanoparticles may enhance the dynamic range and mitigate against deficiencies of BOLD fMRI. At sufficiently high doses the SPIO induced blood T2/T2* reduction effect which overcomes the BOLD effect and the MRI signal that results from neuronal activity becomes predominantly dependent on CBV. CBV fMRI is more attractive for assessing neuronal activity as it renders directly interpretable physiological measurements (142).

Qiu *et al.* (142) reported use of SPIOs in humans demonstrated increased contrast-to-noise ratio (CNR) for neural activation during a unilateral finger tapping task for CBV fMRI with ferumoxytol (510 mg Fe) compared with BOLD fMRI. Baumgartner *et al.* (132) reported in eight

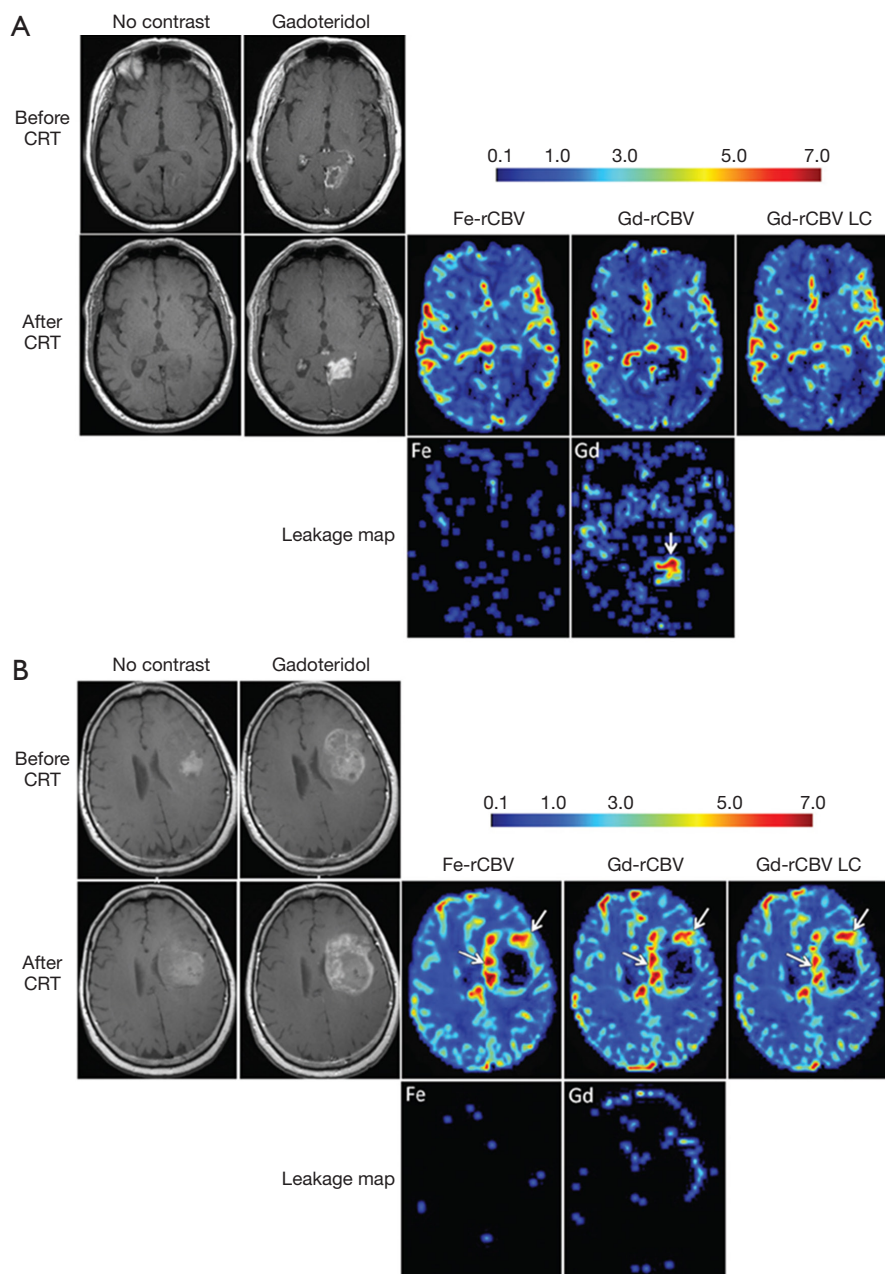


Figure 18 Ferumoxytol enhanced MRI facilitates differentiation between brain tumor progression and pseudoprogession. (A) MR images of a patient with glioblastoma multiforme show pseudoprogession of disease. T1-weighted MR images without contrast enhancement and with gadoteridol obtained before and 3 months after chemoradiotherapy show increased contrast enhancement after treatment. Low rCBV (<1.75) is apparent on parametric maps obtained by using ferumoxytol (Fe-rCBV), gadoteridol (Gd-rCBV), and gadoteridol with leakage correction (Gd-rCBV LC), which indicates pseudoprogession. Leakage map shows absence of contrast extravasation when ferumoxytol (Fe) was used and contrast leakage with gadoteridol (arrow); (B) MR images of a patient with glioblastoma multiforme show progression of disease. T1-weighted MR images without contrast agent and with gadoteridol (Gd) obtained before and 2 weeks after chemoradiotherapy show increased contrast enhancement after treatment. High rCBV (>1.75) is apparent on parametric maps obtained by using ferumoxytol (Fe-rCBV), gadoteridol (Gd-rCBV), and gadoteridol with leakage correction (Gd-rCBV LC), which indicates true tumor progression (arrows). No contrast agent extravasation is seen on leakage map with Fe but small leakage in the lateral aspect of the tumor is seen with gadoteridol [Reprinted with permission (140)].

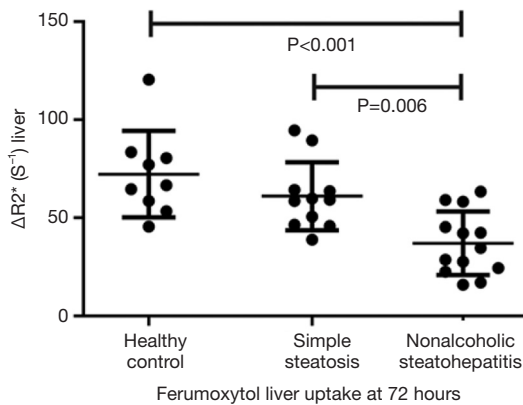


Figure 19 Plot of liver Ferumoxytol uptake. Patients with NASH have decreased hepatic Ferumoxytol uptake, as reflected by a lower delta R2* 72 hours after Ferumoxytol infusion compared with patients with simple steatosis and healthy control subjects [Reprinted with permission (147)].

subjects BOLD and CBV were acquired in response to a visual black-and-white check board stimulation paradigm using an escalating ferumoxytol dose design (250, 350, and 510 mg Fe). It was reported that CBV fMRI techniques and endpoints are dose dependent, and have good test-retest repeatability, and SPIO enhances sensitivity of fMRI stimulus-response endpoints.

Other selected applications of ferucarbotran and ferumoxytol

Florian *et al.* (146) reported the safety profile and potential “therapeutic” effect of intravenous ferumoxytol-based iron administration regarding infarct healing in patients with ST-elevation myocardial infarction. Intravenous iron administration in acute ST-elevation myocardial infarction patients seems to be associated with an improved infarct healing and a beneficial global left ventricular remodelling. The immunomodulatory effect makes USPIO-based iron administration a very attractive candidate as a “diagnostic” and “therapeutic” adjunctive solution in acute MI management. More confirmatory studies are awaited for such a highly attractive concept.

Nonalcoholic fatty liver disease (NAFLD) comprises a spectrum of disease states, including simple steatosis, nonalcoholic steatohepatitis (NASH), hepatic fibrosis, and hepatic cirrhosis. Whereas simple steatosis is considered a benign condition, NASH represents a threatening disease in view of its potential progression to fibrosis and cirrhosis in

up to 30% of cases. Differentiation between simple steatosis and NASH bears direct prognostic implications and, in the light of emerging therapies for NASH, therapeutic consequences for individual patients. Smits *et al.* (147) reported at 3T hepatic uptake of ferumoxytol in patients with NASH is decreased, and group-wise show difference in deltaR2* (= contrast-enhanced R2* value—baseline R2* value) from that of simple steatosis. Patients with NASH had a significantly lower deltaR2* 72 hours after ferumoxytol administration (a dose of 3.6 mg/kg of lean body mass) when compared with patients who had simple steatosis and healthy control subjects (mean \pm standard deviation for patients with NASH, 37.0 \pm 16.1 sec⁻¹; patients with simple steatosis, 61.0 \pm 17.3 sec⁻¹; and healthy control subjects, 72.2 \pm 22.0 sec⁻¹) (Figure 19).

X-ray fluoroscopy and digital subtraction angiography (DSA) is the currently the current gold standard in guidance of vascular interventions. Drawbacks of X-ray based technology include exposure of patients and physicians to ionizing radiation, use of nephrotoxic iodinated contrast agents, the lack of real time three-dimensional imaging. Magnetic particle imaging (MPI) uses the nonlinear magnetization curve of SPIO particles for signal generation. One key characteristic and fundamental difference of MPI compared with other imaging modalities is the high magnetic moment (about 108 times higher than protons) and the fast relaxivity (about 104 times faster than protons in water) of SPIOs (148,149). In the framework of the Magnetic Particle Imaging Technology consortium, funded by the German Federal Ministry of Education and Research, the University of Lübeck and Philips Technology Innovative Technologies (Hamburg, Germany) created a cooperation initiative to develop this technique (150). MPI depicts the spatial distribution of SPIO particles by using oscillating magnetic fields. MPI’s signal strength is proportional to the SPIOs’ concentration over a wide range of practically relevant concentrations. Haegele *et al.* (151,152) reported an approach to visualize a commercially available diagnostic catheter and guide wire for use in MPI guided vascular interventions using a very thin Resovist-coating and a dedicated MPI system. Haegele *et al.* (150) reported that by using MPI, both balloon catheters could be visualized with high temporal resolution and sufficient spatial resolution (Figure 20).

Kakite *et al.* (153) evaluated the usefulness of administration of Resovist and MRI for assessing the efficacy of radiofrequency liver ablation. They reported that the administration of SPIO made it possible to precisely

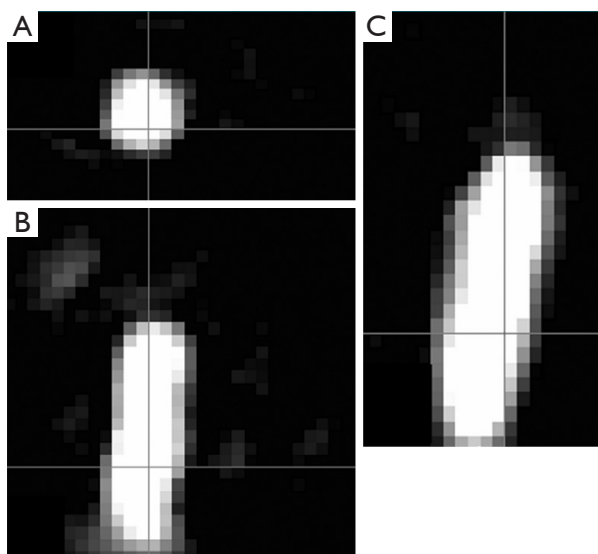


Figure 20 (A) Axial, (B) sagittal, and (C) coronal MP images show Ferucarbotran-labeled balloon catheter. The catheter is delineable in the 3-dimensional FOV of $20 \times 36 \times 36 \text{ mm}^3$ [Reprinted with permission (150)].

evaluate ablated liver parenchyma by hypointense rim on T2* images. This method is helpful for the evaluation of safety margin after radiofrequency ablation for liver tumors.

At the time of writing this review, the Clinicaltrials.gov website showed that currently the total number of open studies involving ferumoxytol was 22, involving around 1,240 patients in five countries. Main indications including brain tumours: 4 studies, 387 patients; MR angiography: 2 studies, 50 patients; lymph node imaging: 3 studies, 104 patients (esophagus and stomach: 2 studies, bladder/prostate/kidney: 1 study); Cardiology: 3 studies, 230 patients ; Bone: 2 studies, 70 patients ; Brain inflammation (not tumoral): 1 study, 30 patients.

Other selected studies of experimental SPIO agents

Cheng *et al.* (154) reported curcumin-conjugated SPIO for detecting amyloid plaques in Alzheimer's disease transgenic mice brain using MRI. Curcumin is a natural product extracted from turmeric, the root of the *Curcuma longa* plant. Curcumin demonstrated safety in human clinical trials. Additionally, it possesses the ability to bind both amyloid β plaques and iron by different regions of the molecule. Cheng *et al.* (154) developed a novel curcumin-conjugated SPIO stabilized by amphiphilic block copolymer (PEG-PLA). This

curcumin magnetic nanoparticles (Cur-SPIO, or Cur-MNP) have a mean diameter $<100 \text{ nm}$ (Figure 21).

The Cur-SPIO particles exhibit brain blood barrier (BBB) penetration potential in an *in vitro* monolayer cell permeability test. *In vivo*, the particles can penetrate the BBB of both Tg2576 Alzheimer's disease model and non-transgenic mice brain. Cur-SPIO binds amyloid plaques in mouse brains, as shown by multiple detection methods (154). T2* *ex vivo* MRI reveals more dark spots in transgenic mice than control mice (Figure 20). Many of the dark spots aligned with amyloid plaques on immunohistochemically stained sections matched with magnetic resonance images. Iron staining, fluorescence, and immunohistochemistry revealed co-localization of SPIO and Curcumin on amyloid plaques (Figure 22). The possible mechanisms by which Cur-SPIO reaches the brain may include Cur-SPIO penetrating BBB endothelial cells by transcytosis. Another possible mechanism is transcytosis, which is facilitated by properties of Cur-SPIO including their small size and their PEG layer, which prolongs blood circulation and which interacts with BBB endothelial cells. It is expected that it will be more sensitive if Cur-SPIO and susceptibility weighted imaging are combined together to image amyloid beta plaque (155-157). Therefore Cur-SPIO may have the potential use for visualizing amyloid plaques in Alzheimer's disease patients. Of note, Curcumin has also been conjugated to Gd-DOTA for amyloid beta plaques detection (158). The dilemma for such probe will be that the clinical need is not strong in the absence of effective drugs; however, it may help the development of such drugs.

Another very interesting type of SPIO has been recently developed by a Japanese group (159-161). In order to improve the properties for the applications such as drug targeting and tissue or organ imaging other than liver, it is extremely important to avoid the nonspecific uptake of SPIO by peripheral macrophages as well as by mononuclear phagocyte system and RES. Ohno *et al.* (159) reported that their synthetic technique renders the SPIO particle stealthy so that only very limited amounts are absorbed by phagocytes. They fabricated hybrid particles composed of a core of Fe_3O_4 nanoparticle and a shell coating of concentrated hydrophilic polymer brushes. The polymer brushes are composed by hydrophilic polymers, poly [poly (ethylene glycol) methyl ether methacrylate (PEGMA)] (159,160). The mean hydrodynamic diameter of this particle is 100 nm. This new hydrophilic SPIO probe showed dispersibility in aqueous media and a marked increase in blood circulation time due to its stealth characteristics, and

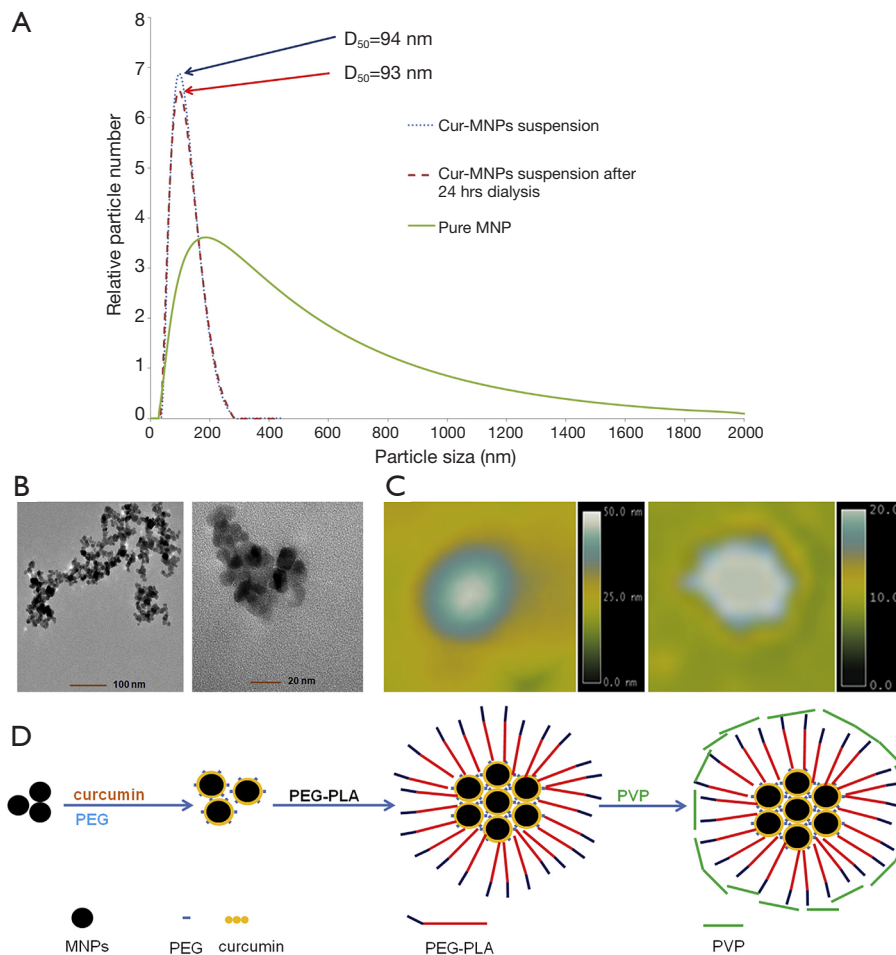


Figure 21 Particle size characterizations of Cur-MNP. (A) Sizes of pure SPIO and Cur-SPIO (freshly made and after 24 h dialysis) measured by dynamic light scattering analyzer; (B) TEM images of pure SPIO (left) and Cur-SPIO (right); (C) AFM images of a Cur-SPIO in morphology mode (left) and in phase difference mode (right); (D) Step-wise process of making Cur-SPIO [Reprinted with permission (154)]. SPIO, superparamagnetic iron oxide; Cur-MNP, Curcumin SPIO nanoparticles.

are almost not taken by phagocytes due to the suppression of non-specific protein binding caused by their “brush-afforded” structure. Though the new SPIO was absorbed in only negligible amounts by phagocytes in liver and lymphatic tissues due to its stealth behavior, numerous particles were engulfed by mesangial cells in kidney glomeruli. Additionally, transmission electron microscopy revealed that Ferucarbotran and the new SPIO accumulated in different cells of glomeruli, that is, endothelial and mesangial cells, respectively. The unique distribution of the new SPIO in normal mesangial cells may have the potential to be used as a marker to assess the glomerular function of kidney (161).

Opportunities and challenges for clinical development of SPIO agents.

Despite some SPIO agents have been approved by regulatory bodies for many years, the up-take and usage in clinical practice have been proven a difficult journey (4,5). Particularly, Feridex[®] has to be taken out of market due to lack of users. Ferucarbotran (Resovist[®]) remains available only in a limited number of countries. These constitute huge revenue loss for the developers (pharmaceutical companies). SPIO agents have to compete with the fast technological progress of MRI (5), as well as competitor agents such as Gd-EOB-DTPA (Primovist[®]); while as usual, process of

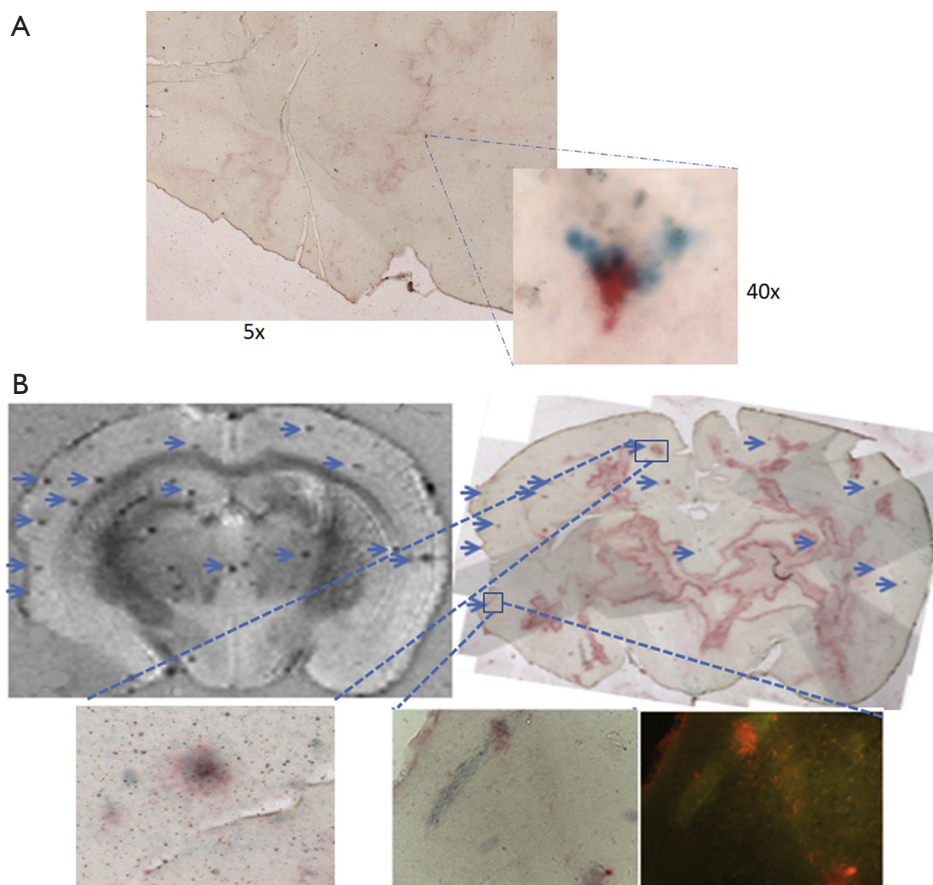


Figure 22 Iron staining, fluorescence, and immunohistochemistry reveal co-localization of SPIO and Curcumin on amyloid plaques. (A) Bright view of histochemically labeled Alzheimer's disease transgenic mouse brain section. Immunohistochemically labeled amyloid plaques (red) and Prussian blue stained iron oxide (blue). Inset: 40x magnification of a region displaying co-localization of iron oxide with a plaque; (B) match between the black dots of 7 Tesla MRI (left) and plaques labeled immunohistochemically (red) and by Cur-SPIO (blue). Left inset: iron (blue) anchored on plaques (red). Right inset: curcumin (fluorescent) co-localization on the plaques. Insets: 100x magnification of plaques [Reprinted with permission (154)]. SPIO, superparamagnetic iron oxide.

clinical trials and regulatory approval are very slow (10), which otherwise would have constituted opportunities including the time window before the approval of Gd-EOB-DTPA. The clinical take-up of Feridex[®] and Resovist[®], and the withdrawal of ferumoxtran-10 filing are further hindered by the following facts; and proactive steps should be taken to address them.

(I) The vast majority of radiologists and other diagnostic physicians have little experience in interpreting SPIO enhanced MR images. This lead to radiologists and other diagnostic physicians are reluctant to order an SPIO enhanced examination even when such an option is available. In the future, this obstacle may be overcome by tele-radiology

and data are sent to central reading facilities staffed by radiologists with expertise in interpreting SPIO enhanced MR images; or patients can visit centers of excellence for SPIO enhanced MRI examination and interpretation (such as the Prostate MR-Center of Excellence at Nijmegen, the Netherlands). Educational courses, educational websites, or tele-radiology sponsored or managed by SPIO developers may help on this matter;

(II) The measurement of the extent of SPIO enhancement is often quantified by measurement of T2*relaxation and delta T2* (difference of T2* relaxation before and after SPIO enhancement), and delta T2* is assumed to correlated to the amount of

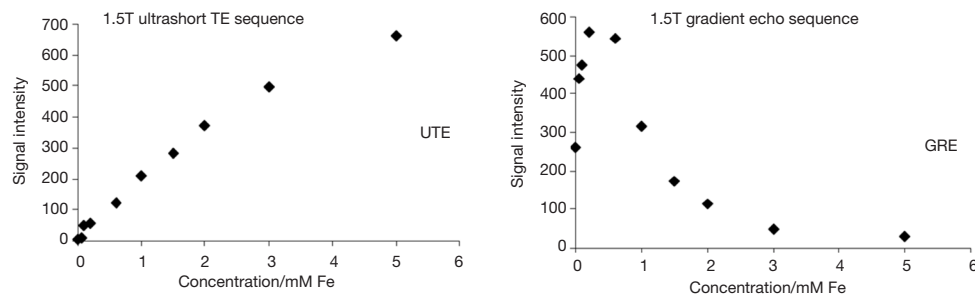


Figure 23 There is a close to linear correlation between signal intensity and concentration by UTE (ultrashort TE). Whereas with gradient echo the signal intensity relationship is complex with an initial increase from T1 effects and T2* causing signal decrease at concentrations >0.2 mM [Reprinted with permission (93)].

SPIO. However, this T2* is prone to measurement inaccuracy influenced by, among others, magnetic field B0 inhomogeneities. Further MR technology development to improve T2* quantification accuracy and consistency is important and is expected to be feasible (162-164). Another possibility will be to exploit the T1 relaxation enhancement of SPIO by T1 weighted MR sequences, and therefore the positive (bright) enhancement of SPIO (162,165). The further wider use of quantitative susceptibility mapping (QSM) or wider spread of even higher magnetic strength such as 7 Tesla is likely both to reduce the required dosage of SPIO agents as well as the quantification accuracy of local iron concentration. The relationship between $\Delta T2^*$ and concentration of iron is more likely to be linear when the iron concentration is low. Moreover, it has been noted that ultra-short TE (UTE) enhancement shows a close to linear relationship to SPIO concentration (93) (Figure 23). The authors believe further development of MRI technology including better quantification and higher resolution, and made them widely available in clinical scanners, is vital for the further managed application of SPIO/USPIO (166-168);

- (III) To get an agent approved, the regulatory bodies or health authorities not only request the rigorous demonstration of the proof of concept, but also of improved patient outcome. This requirement is often for the insurance coverage as well. The one-off use of contrast agents for imaging examination, as compared with in many cases long-term (months or even years) use of therapeutic agents, means

the financial return for contrast agents is often much smaller, unless the contrast agent is used in large volume in many patients (such as iodinated contrast agents, or Gd-DTPA, Gd-DOTA etc.). On the other hand, the clinical development costs for contrast agents can be roughly similar (or slightly less than) to therapeutic agents. From the pharmaceutical industry's perspective, an important obstacle is that the projected volume of SPIO usage is not particularly large. For example, SPIO-enhanced MR angiography will be used in patients with compromised renal function and unsuitable for CT or MR angiography using linear GBCA or iodinated agents. Ferumoxytol is not currently clinically indicated for imaging. Till it is approved for imaging, the application can be only off-label, and there will be the issue of reimbursement, insurance and the physicians bear the safety concerns. Contrast agent developers are concerned with the huge risk of refusal from the health authorities, and no obvious guarantee that, if marketed, the clinical diagnosticians will adopt them. Such as even if the compound had proofs of concept and saved life; as ferumoxtran-10 for lymph node imaging in prostate cancer, market access chance remains quite poor till now. The selection of clinical indications is also an important topic to consider. For example, the low return on investment/regulatory requirement ratio anticipated for the imaging of stem cell migration and immune cell trafficking indication probably explains why little industrial effort has been made in this field (8). On the other hand, some clinicians

who investigated USPIOs such as Dr. Barentsz's team at University of Nijmegen, the Netherlands, are convinced of their clinical value to the point that they decided to develop ferumoxtran-10 on their own;

- (IV) Cross-center and inter-center validation of SPIO enhanced MRI readout should be better coordinated. Clinical data should be systematically synthesized and regularly updated. An 'open science' may facilitate the approval of some 'orphan applications' of SPIO; and novel applications of SPIO should be continuously explored.

Literatures in the past 5 years show clinical research on SPIO remains robust, particularly fuelled by the approval of ferumoxytol for intravenous infusion, though with the limitation of safety concerns and currently not available in EU because of this reason for anemia indication. To further develop SPIO agents for clinical application, improvement of MR technique and image post-processing may be important so to allow accurate and reliable quantification of SPIO enhancement and SPIO concentration in the targeted tissues/organs. Central reading facility with the help of tele-radiology technologies or dedicated centers of excellence may allow improved and consistent interpretation of SPIO enhanced MR images. Overall, much more research is required to firmly establish the true value of SPIO against the false positive /false negative risks, as well as the safety profile of SPIOs at various dosages.

Acknowledgements

We like to thank Prof Chenjie Xu of Nanyang Technological University, Singapore; and Prof Weitian Chen of the Chinese University of Hong Kong, Hong Kong SAR, for critical comments of this manuscript; and thank Mr Jun-Qing Wang MSc (biotech) for proof-reading of the manuscript.

Funding: Author (YXJW) acknowledges the funding support of direct grant for research from the Chinese University of Hong Kong (No. 4054167).

Footnote

Conflicts of Interest: JM Idée is an employee of Guerbet group, France. Guerbet group manufactures and markets a number of contrast agents for diagnostic and interventional imaging. And other author has no conflicts of interest to declare.

References

1. Wang YX, Xuan S, Port M, Idee JM. Recent advances in superparamagnetic iron oxide nanoparticles for cellular imaging and targeted therapy research. *Curr Pharm Des* 2013;19:6575-93.
2. Wang YX, Hussain SM, Krestin GP. Superparamagnetic iron oxide contrast agents: physicochemical characteristics and applications in MR imaging. *Eur Radiol* 2001;11:2319-31.
3. Wang YX, Idee JM, Corot C. Scientific and industrial challenges of developing nanoparticle-based theranostics and multiple-modality contrast agents for clinical application. *Nanoscale* 2015;7:16146-50.
4. Wang YX. Chapter 2: Superparamagnetic iron oxide particle nanoparticles for cellular imaging and targeted therapy: Opportunities and changes for clinical translation. In: Zhang B. editor. *Nano Imaging: From fundamental Principles to Translational Medical Applications*. Singapore: World Scientific, 2017:29-51.
5. Wang YX. Current status of superparamagnetic iron oxide contrast agents for liver magnetic resonance imaging. *World J Gastroenterol* 2015;21:13400-2.
6. Schleich N, Danhier F, Pr eat V. Iron oxide-loaded nanotheranostics: Major obstacles to in vivo studies and clinical translation. *J Control Release* 2015;198:35-54.
7. Dassler K, Roohi F, Lohrke J, Ide A, Remmele S, H utter J, Pietsch H, Pison U, Sch utz G. Current limitations of molecular magnetic resonance imaging for tumors as evaluated with high-relaxivity CD105-specific iron oxide nanoparticles. *Invest Radiol* 2012;47:383-91.
8. Id e JM, Louguet S, Ballet S, Corot C. Theranostics and contrast-agents for medical imaging: a pharmaceutical company viewpoint. *Quant Imaging Med Surg* 2013;3:292-7.
9. Wang YX, Choi Y, Chen Z, Laurent S, Gibbs SL. Molecular imaging: from bench to clinic. *Biomed Res Int* 2014;2014:357258.
10. Wang YX. Medical imaging in pharmaceutical clinical trials: what radiologists should know. *Clin Radiol* 2005;60:1051-7.
11. Choi HS, Frangioni JV. Nanoparticles for biomedical imaging: fundamentals of clinical translation. *Mol Imaging* 2010;9:291-310.
12. Corot C, Warlin D. Superparamagnetic iron oxide nanoparticles for MRI: contrast media pharmaceutical company R&D perspective. *Wiley Interdiscip Rev Nanomed Nanobiotechnol* 2013;5:411-22.

13. Wáng YX. Systematic review and meta-analysis of diagnostic imaging technologies. *Quant Imaging Med Surg* 2016;6:615-8.
14. Vasanawala SS, Nguyen KL, Hope MD, Bridges MD, Hope TA, Reeder SB, Bashir MR. Safety and technique of ferumoxytol administration for MRI. *Magn Reson Med* 2016;75:2107-11.
15. Kim JE, Shin JY, Cho MH. Magnetic nanoparticles: an update of application for drug delivery and possible toxic effects. *Arch Toxicol* 2012;86:685-700.
16. Santosh S, Podaralla P, Miller B. Anaphylaxis with elevated serum tryptase after administration of intravenous ferumoxytol. *NDT Plus* 2010;3:341-2.
17. Bailie GR. Comparison of rates of reported adverse events associated with i.v. iron products in the United States. *Am J Health Syst Pharm* 2012;69:310-20.
18. Pai AB, Garba AO. Ferumoxytol: a silver lining in the treatment of anemia of chronic kidney disease or another dark cloud? *J Blood Med* 2012;3:77-85.
19. Muehe AM, Feng D, von Eyben R, Luna-Fineman S, Link MP, Muthig T, Huddleston AE, Neuwelt EA, Daldrup-Link HE. Safety Report of Ferumoxytol for Magnetic Resonance Imaging in Children and Young Adults. *Invest Radiol* 2016;51:221-7.
20. Food_and_Drug_Administration. Feraheme Package Insert. Available online: http://www.accessdata.fda.gov/drugsatfda_docs/label/2009/022180lbl.pdf
21. Food_and_Drug_Administration. Isovue Package Insert. Available online: http://www.accessdata.fda.gov/drugsatfda_docs/label/2012/018735s054lbl.pdf
22. McCulley L, Gelperin K, Bird S, Harris S, Wang C, Waldron P. Reports to FDA of fatal anaphylaxis associated with intravenous iron products. *Am J Hematol* 2016;91:E496-E497.
23. Chang YK, Liu YP, Ho JH, Hsu SC, Lee OK. Amine-surface-modified superparamagnetic iron oxide nanoparticles interfere with differentiation of human mesenchymal stem cells. *J Orthop Res* 2012;30:1499-506.
24. Cromer Berman SM, Kshitiz C, Wang J, Orukari I, Levchenko A, Bulte JW, Walczak P. Cell motility of neural stem cells is reduced after SPIO-labeling, which is mitigated after exocytosis. *Magn Reson Med* 2013;69:255-62.
25. Wáng YX. Superparamagnetic iron oxide based MRI contrast agents: Current status of clinical application. *Quant Imaging Med Surg* 2011;1:35-40.
26. Corot C, Robert P, Idée JM, Port M. Recent advances in iron oxide nanocrystal technology for medical imaging. *Adv Drug Deliv Rev* 2006;58:1471-1504.
27. Klein C, Nagel E, Schnackenburg B, Bornstedt A, Schalla S, Hoffmann V, Lehning A, Fleck E. The intravascular contrast agent Clariscan (NC 100150 injection) for 3D MR coronary angiography in patients with coronary artery disease. *MAGMA* 2000;11:65-7.
28. Wagner M, Wagner S, Schnorr J, Schellenberger E, Kivelitz D, Krug L, Dewey M, Laule M, Hamm B, Taupitz M. Coronary MR angiography using citrate-coated very small superparamagnetic iron oxide particles as blood-pool contrast agent: initial experience in humans. *J Magn Reson Imaging* 2011;34:816-23.
29. Polakova K, Mocikova I, Purova D, Tucek P, Novak P, Novotna K, Izak N, Bielik R, Zboril R, Miroslav H. Magnetic resonance cholangiopancreatography (MRCP) using new negative per-oral contrast agent based on superparamagnetic iron oxide nanoparticles for extrahepatic biliary duct visualization in liver cirrhosis. *Biomed Pap Med Fac Univ Palacky Olomouc Czech Repub* 2016;160:512-7.
30. Bashir MR, Bhatti L, Marin D, Nelson RC. Emerging applications for ferumoxytol as a contrast agent in MRI. *J Magn Reson Imaging* 2015;41:884-98.
31. Albaramki J, Hodson EM, Craig JC, Webster AC. Parenteral versus oral iron therapy for adults and children with chronic kidney disease. *Cochrane Database Syst Rev* 2012;1:CD007857.
32. McCullough BJ, Kolokythas O, Maki JH, Green DE. Ferumoxytol in clinical practice: implications for MRI. *J Magn Reson Imaging* 2013;37:1476-9.
33. Schieda N. Parenteral ferumoxytol interaction with magnetic resonance imaging: a case report, review of the literature and advisory warning. *Insights Imaging* 2013;4:509-12.
34. Gunn AJ, Seethamraju RT, Hedgire S, Elmi A, Daniels GH, Harisinghani MG. Imaging behavior of the normal adrenal on ferumoxytol-enhanced MRI: preliminary findings. *AJR Am J Roentgenol* 2013;201:117-21.
35. Storey P, Arbini AA. Bone marrow uptake of ferumoxytol: a preliminary study in healthy human subjects. *J Magn Reson Imaging* 2014;39:1401-10.
36. Harisinghani MG, Barentsz J, Hahn PF, Deserno WM, Tabatabaei S, van de Kaa CH, de la Rosette J, Weissleder R. Noninvasive detection of clinically occult lymph-node metastases in prostate cancer. *N Engl J Med* 2003;348:2491-9.
37. European Medicines Agency. Withdrawal assessment report for sinerem. Available online: <http://www.qims.amegroups.com>

- ema.europa.eu/docs/en_GB/document_library/Application_withdrawal_assessment_report/2010/01/WC500067463.pdf
38. Fortuin AS, Smeenk RJ, Meijer HJ, Witjes AJ, Barentsz JO. Lymphotropic nanoparticle-enhanced MRI in prostate cancer: value and therapeutic potential. *Curr Urol Rep* 2014;15:389.
 39. Broome DR, Girguis MS, Baron PW, Cottrell AC, Kjellin I, Kirk GA. Gadodiamide-associated nephrogenic systemic fibrosis: why radiologists should be concerned. *AJR Am J Roentgenol* 2007;188:586-92.
 40. Grobner T. Gadolinium—a specific trigger for the development of nephrogenic fibrosing dermopathy and nephrogenic systemic fibrosis? *Nephrol Dial Transplant* 2006;21:1104-8.
 41. Sadowski EA, Bennett LK, Chan MR, Wentland AL, Garrett AL, Garrett RW, Djamali A. Nephrogenic systemic fibrosis: risk factors and incidence estimation. *Radiology* 2007;243:148-57.
 42. Wáng YX, Schroeder J, Siegmund H, Idée JM, Fretellier N, Jestin-Mayer G, Factor C, Deng M, Kang W, Morcos SK. Total gadolinium tissue deposition and skin structural findings following the administration of structurally different gadolinium chelates in healthy and ovariectomized female rats. *Quant Imaging Med Surg* 2015;5:534-45.
 43. Schwein A, Chinnadurai P, Shah DJ, Lumsden AB, Bechara CF, Bismuth J. Feasibility of three-dimensional magnetic resonance angiography-fluoroscopy image fusion technique in guiding complex endovascular aortic procedures in patients with renal insufficiency. *J Vasc Surg* 2016. [Epub ahead of print]. doi: 10.1016/j.jvs.2016.10.083.
 44. Schubert T, Motosugi U, Kinner S, Colgan TJ, Sharma SD, Hetzel S, Wells S, Campo CA, Reeder SB. Crossover comparison of ferumoxytol and gadobenate dimeglumine for abdominal MR-angiography at 3.0 tesla: Effects of contrast bolus length and flip angle. *J Magn Reson Imaging* 2016. [Epub ahead of print]. doi: 10.1002/jmri.25513.
 45. Zhou Z, Han F, Rapacchi S, Nguyen KL, Brunengraber DZ, Kim GJ, Finn JP, Hu P. Accelerated ferumoxytol-enhanced 4D multiphase, steady-state imaging with contrast enhancement (MUSIC) cardiovascular MRI: validation in pediatric congenital heart disease. *NMR Biomed* 2017;30. [Epub ahead of print]. doi: 10.1002/nbm.3663
 46. Lai LM, Cheng JY, Alley MT, Zhang T, Lustig M, Vasanawala SS. Feasibility of ferumoxytol-enhanced neonatal and young infant cardiac MRI without general anesthesia. *J Magn Reson Imaging* 2016. [Epub ahead of print]. doi: 10.1002/jmri.25482
 47. Luhar A, Khan S, Finn JP, Ghahremani S, Griggs R, Zaritsky J, Salusky I, Hall TR. Contrast-enhanced magnetic resonance venography in pediatric patients with chronic kidney disease: initial experience with ferumoxytol. *Pediatr Radiol* 2016;46:1332-40.
 48. Ning P, Zucker EJ, Wong P, Vasanawala SS. Hemodynamic safety and efficacy of ferumoxytol as an intravenous contrast agents in pediatric patients and young adults. *Magn Reson Imaging* 2016;34:152-8.
 49. Sigovan M, Gasper W, Alley HF, Owens CD, Saloner D. USPIO-enhanced MR angiography of arteriovenous fistulas in patients with renal failure. *Radiology* 2012;265:584-90.
 50. Ersoy H, Jacobs P, Kent CK, Prince MR. Blood pool MR angiography of aortic stent-graft endoleak. *AJR Am J Roentgenol* 2004;182:1181-6.
 51. Cochran AJ, Essner R, Rose DM, Glass EC. Principles of sentinel lymph node identification: background and clinical implications. *Langenbecks Arch Surg* 2000;385:252-60.
 52. Bézu C, Coutant C, Salengro A, Daraï E, Rouzier R, Uzan S. Anaphylactic response to blue dye during sentinel lymph node biopsy. *Surg Oncol* 2011;20: e55-e59.
 53. Motomura K, Ishitobi M, Komoike Y, Koyama H, Noguchi A, Sumino H, Kumatani Y, Inaji H, Horinouchi T, Nakanishi K. SPIO-enhanced magnetic resonance imaging for the detection of metastases in sentinel nodes localized by computed tomography lymphography in patients with breast cancer. *Ann Surg Oncol* 2011;18:3422-9.
 54. Motomura K, Izumi T, Tateishi S, Sumino H, Noguchi A, Horinouchi T, Nakanishi K. Correlation between the area of high-signal intensity on SPIO-enhanced MR imaging and the pathologic size of sentinel node metastases in breast cancer patients with positive sentinel nodes. *BMC Med Imaging* 2013;13:32.
 55. Shiozawa M, Kobayashi S, Sato Y, Maeshima H, Hozumi Y, Lefor AT, Kurihara K, Sata N, Yasuda Y. Magnetic resonance lymphography of sentinel lymph nodes in patients with breast cancer using superparamagnetic iron oxide: a feasibility study. *Breast Cancer* 2014;21:394-401.
 56. Motoyama S, Ishiyama K, Maruyama K, Narita K, Minamiya Y, Ogawa J. Estimating the need for neck lymphadenectomy in submucosal esophageal cancer using superparamagnetic iron oxide-enhanced magnetic resonance imaging: clinical validation study. *World J Surg* 2012;36:83-9.

57. Motomura K, Izumi T, Tateishi S, Tamaki Y, Ito Y, Horinouchi T, Nakanishi K. Superparamagnetic iron oxide-enhanced MRI at 3 T for accurate axillary staging in breast cancer. *Br J Surg* 2016;103:60-9.
58. Kuijs VJ, Moosdorff M, Schipper RJ, Beets-Tan RG, Heuts EM, Keymeulen KB, Smidt ML, Lobbes MB. The role of MRI in axillary lymph node imaging in breast cancer patients: a systematic review. *Insights Imaging* 2015;6:203-15.
59. Mizokami D, Kosuda S, Tomifuji M, Araki K, Yamashita T, Shinmoto H, Shiotani A. Superparamagnetic iron oxide-enhanced interstitial magnetic resonance lymphography to detect a sentinel lymph node in tongue cancer patients. *Acta Otolaryngol* 2013;133:418-23.
60. Maki JH, Neligan PC, Briller N, Mitsumori LM, Wilson GJ. Dark Blood Magnetic Resonance Lymphangiography Using Dual-Agent Relaxivity Contrast (DARC-MRL): A Novel Method Combining Gadolinium and Iron Contrast Agents. *Curr Probl Diagn Radiol* 2016;45:174-9.
61. Will O, Purkayastha S, Chan C, Althanasios T, Darzi AW, Gedroyc W, Tekkis PP. Diagnostic precision of nanoparticle-enhanced MRI for lymph-node metastases: a meta-analysis. *Lancet Oncol* 2006;7:52-60.
62. Harnan SE, Cooper KL, Meng Y, Ward SE, Fitzgerald P, Papaioannou D, Ingram C, Lorenz E, Wilkinson ID, Wyld L. Magnetic resonance for assessment of axillary lymph node status in early breast cancer: a systematic review and meta-analysis. *Eur J Surg Oncol* 2011;37:928-36.
63. Meng Y, Ward S, Cooper K, Harnan S, Wyld L. Cost effectiveness of MRI and PET imaging for the evaluation of axillary lymph node metastases in early stage breast cancer. *Eur J Surg Oncol* 2011;37:40-6.
64. Minamiya Y, Ito M, Katayose Y, Saito H, Imai K, Sato Y, Ogawa J. Intraoperative sentinel lymph node mapping using a new sterilizable magnetometer in patients with nonsmall cell lung cancer. *Ann Thorac Surg* 2006;81:327-30.
65. Imai K, Kawaharada Y, Ogawa J, Saito H, Kudo S, Takashima S, Saito Y, Atari M, Ito A, Terata K, Yoshino K, Sato Y, Motoyama S, Minamiya Y. Development of a New Magnetometer for Sentinel Lymph Node Mapping Designed for Video-Assisted Thoracic Surgery in Non-Small Cell Lung Cancer. *Surg Innov* 2015;22:401-5.
66. Waanders S, Visscher M, Wildeboer RR, Oderkerk TO, Krooshoop HJ, Ten Haken B. A handheld SPIO-based sentinel lymph node mapping device using differential magnetometry. *Phys Med Biol* 2016;61:8120-34.
67. Shiozawa M, Lefor AT, Hozumi Y, Kurihara K, Sata N, Yasuda Y, Kusakabe M. Sentinel lymph node biopsy in patients with breast cancer using superparamagnetic iron oxide and a magnetometer. *Breast Cancer* 2013;20:223-9.
68. Karakatsanis A, Christiansen PM, Fischer L, Hedin C, Pistioli L, Sund M, Rasmussen NR, Jørnsgård H, Tegnelius D, Eriksson S, Daskalakis K, Wärnberg F, Markopoulos CJ, Bergkvist L. The Nordic SentiMag trial: a comparison of super paramagnetic iron oxide (SPIO) nanoparticles versus Tc(99) and patent blue in the detection of sentinel node (SN) in patients with breast cancer and a meta-analysis of earlier studies. *Breast Cancer Res Treat* 2016;157:281-94.
69. Douek M, Klaase J, Monypenny I, Kothari A, Zechmeister K, Brown D, Wyld L, Drew P, Garmo H, Agbaje O, Pankhurst Q, Anninga B, Grootendorst M, Ten Haken B, Hall-Craggs MA, Purushotham A, Pinder S, SentiMAG Trialists Group. Sentinel node biopsy using a magnetic tracer versus standard technique: the SentiMAG Multicentre Trial. *Ann Surg Oncol* 2014;21:1237-45.
70. Thill M, Kurylcio A, Welter R, van Haasteren V, Grosse B, Berclaz G, Polkowski W, Hauser N. The Central-European SentiMag study: sentinel lymph node biopsy with superparamagnetic iron oxide (SPIO) vs. radioisotope. *Breast* 2014;23:175-9.
71. Rubio IT, Diaz-Botero S, Esgueva A, Rodriguez R, Cortadellas T, Cordoba O, Espinosa-Bravo M. The superparamagnetic iron oxide is equivalent to the Tc99 radiotracer method for identifying the sentinel lymph node in breast cancer. *Eur J Surg Oncol* 2015;41:46-51.
72. Piñero-Madrona A, Torr6-Richart JA, de Le6n-Carrillo JM, de Castro-Parga G, Navarro-Cecilia J, Dom6nguez-Cunchillos F, Rom6n-Santamar6a JM, Fuster-Diana C, Pardo-Garc6a R; Grupo de Estudios Senol6gicos de la Sociedad Espa6ola de Patolog6a Mamaria (SESPM). Superparamagnetic iron oxide as a tracer for sentinel node biopsy in breast cancer: A comparative non-inferiority study. *Eur J Surg Oncol* 2015;41:991-7.
73. Ghilli M, Carretta E, Di Filippo F, Battaglia C, Fustaino L, Galanou I, Di Filippo S, Rucci P, Fantini MP, Roncella M. The superparamagnetic iron oxide tracer: a valid alternative in sentinel node biopsy for breast cancer treatment. *Eur J Cancer Care (Engl)* 2015. [Epub ahead of print]. doi: 10.1111/ecc.12385.
74. Houpeau JL, Chauvet MP, Guillemin F, Bendavid-Athias C, Charitansky H, Kramar A, Giard S. Sentinel lymph node identification using superparamagnetic iron oxide particles versus radioisotope: The French SentiMag feasibility trial. *J Surg Oncol* 2016;113:501-7.

75. Coufal O, Fait V, Lžičářová E, Chrenko V, Žaloudík J. SentiMag--the magnetic detection system of sentinel lymph nodes in breast cancer. *Rozhl Chir* 2015;94:283-8.
76. Pouw JJ, Grootendorst MR, Bezooijen R, Klazen CA, De Bruin WI, Klaase JM, Hall-Craggs MA, Douek M, Ten Haken B. Pre-operative sentinel lymph node localization in breast cancer with superparamagnetic iron oxide MRI: the SentiMAG Multicentre Trial imaging subprotocol. *Br J Radiol* 2015;88:20150634.
77. Wang YX, Wang DW, Zhu XM, Zhao F, Leung KC. Carbon coated superparamagnetic iron oxide nanoparticles for sentinel lymph nodes mapping. *Quant Imaging Med Surg* 2012;2:53-6.
78. Ahmed M, Usiskin SI, Hall-Craggs MA, Douek M. Is imaging the future of axillary staging in breast cancer? *Eur Radiol* 2014;24:288-93.
79. Harisinghani MG, Saksena MA, Hahn PF, King B, Kim J, Torabi MT, Weissleder R. Ferumoxtran-10-enhanced MR lymphangiography: does contrast-enhanced imaging alone suffice for accurate lymph node characterization? *AJR Am J Roentgenol* 2006;186:144-8.
80. Islam T, Harisinghani MG. Overview of nanoparticle use in cancer imaging. *Cancer Biomark* 2009;5:61-7.
81. Heesakkers RA, Hövels AM, Jager GJ, van den Bosch HC, Witjes JA, Raat HP, Severens JL, Adang EM, van der Kaa CH, Fütterer JJ, Barentsz J. MRI with a lymph-node-specific contrast agent as an alternative to CT scan and lymph-node dissection in patients with prostate cancer: a prospective multicohort study. *Lancet Oncol* 2008;9:850-6.
82. Lahaye MJ, Engelen SM, Kessels AG, de Bruïne AP, von Meyenfeldt MF, van Engelshoven JM, van de Velde CJ, Beets GL, Beets-Tan RG. USPIO-enhanced MR imaging for nodal staging in patients with primary rectal cancer: predictive criteria. *Radiology* 2008;246:804-11.
83. Fortuin AS, Deserno WM, Meijer HJ, Jager GJ, Takahashi S, Debats OA, Reske SN, Schick C, Krause BJ, van Oort I, Witjes AJ, Hoogeveen YL, van Lin EN, Barentsz JO. Value of PET/CT and MR lymphography in treatment of prostate cancer patients with lymph node metastases. *Int J Radiat Oncol Biol Phys* 2012;84:712-8.
84. Suzuki D, Yamaguchi M, Furuta T, Okuyama Y, Yoshikawa K, Fujii H. Central high signal in inflammatory swollen lymph nodes on SPIO-enhanced interstitial MR lymphograms: a mimic of lymph node metastasis. *Magn Reson Med Sci* 2012;11:61-3.
85. Triantafyllou M, Studer UE, Birkhäuser FD, Fleischmann A, Bains LJ, Petralia G, Christe A, Froehlich JM, Thoeny HC. Ultrasmall superparamagnetic particles of iron oxide allow for the detection of metastases in normal sized pelvic lymph nodes of patients with bladder and/or prostate cancer. *Eur J Cancer* 2013;49:616-24.
86. Smith JT, Ward J, Guthrie JA, Sheridan MB, Boyes S, Wilson D, Wyatt JI, Treanor D, Robinson PJ. Detection of colorectal metastases in patients being treated with chemotherapy utilising SPIO-MRI: a radiological-pathological study. *Magn Reson Imaging* 2012;30:1446-53.
87. Fortuin AS, Barentsz JO. Comments on Ultrasmall superparamagnetic particles of iron oxide allow for the detection of metastases in normal sized pelvic lymph nodes of patients with bladder and/or prostate cancer, Triantafyllou et al., *European Journal of Cancer*, published online 22 October 2012. *Eur J Cancer* 2013;49:1789-90.
88. Froehlich JM, Triantafyllou M, Fleischmann A, Vermathen P, Thalmann GN, Thoeny HC. Does quantification of USPIO uptake-related signal loss allow differentiation of benign and malignant normal-sized pelvic lymph nodes? *Contrast Media Mol Imaging* 2012;7:346-55.
89. McDermott S, Thayer SP, Fernandez-Del Castillo C, Mino-Kenudson M, Weissleder R, Harisinghani MG. Accurate prediction of nodal status in preoperative patients with pancreatic ductal adenocarcinoma using next-gen nanoparticle. *Transl Oncol* 2013;6:670-5.
90. Turkbey B, Agarwal HK, Shih J, Bernardo M, McKinney YL, Daar D, Griffiths GL, Sankineni S, Johnson L, Grant KB, Weaver J, Rais-Bahrami S, Harisinghani M, Jacobs P, Dahut W, Merino MJ, Pinto PA, Choyke PL. A Phase I Dosing Study of Ferumoxytol for MR Lymphography at 3 T in Patients With Prostate Cancer. *AJR Am J Roentgenol* 2015;205:64-9.
91. Atri M, Zhang Z, Marques H, Gorelick J, Harisinghani M, Sohaib A, Koh DM, Raman S, Gee M, Choi H, Landrum L, Mannel R, Chuang L, Yu JQ, McCourt CK, Gold M. Utility of preoperative ferumoxtran-10 MRI to evaluate retroperitoneal lymph node metastasis in advanced cervical cancer: Results of ACRIN 6671/GOG 0233. *Eur J Radiol Open* 2015;2:11-8.
92. Wang YX, Lam WW. Characterisation of brain disorders and evaluation of therapy by functional and molecular magnetic resonance techniques. *Hong Kong Med J* 2008;14:469-78.
93. Crowe LA, Wang YX, Gatehouse P, Tessier J, Waterton J, obert R, Bydder G, Firmin DN. Ex vivo MR imaging of atherosclerotic rabbit aorta labeled with USPIO-enhancement of iron loaded regions in UTE imaging. *Proc Intl Soc Mag Reson Med* 2005:115. Available online:

- <http://cds.ismrm.org/ismrm-2005/Files/00115.pdf>
94. Tourdias T, Roggerone S, Filippi M, Kanagaki M, Rovaris M, Miller DH, Petry KG, Brochet B, Pruvo JP, Radüe EW, Dousset V. Assessment of disease activity in multiple sclerosis phenotypes with combined gadolinium- and superparamagnetic iron oxide-enhanced MR imaging. *Radiology* 2012;264:225-33.
 95. Crimi A, Commowick O, Maarouf A, Ferré JC, Bannier E, Tourbah A, Berry I, Ranjeva JP, Edan G, Barillot C. Predictive value of imaging markers at multiple sclerosis disease onset based on gadolinium- and USPIO-enhanced MRI and machine learning. *PLoS One* 2014;9:e93024.
 96. Maarouf A, Ferré JC, Zaaoui W, Le Troter A, Bannier E, Berry I, Guye M, Pierot L, Barillot C, Pelletier J, Tourbah A, Edan G, Audoin B, Ranjeva JP. Ultra-small superparamagnetic iron oxide enhancement is associated with higher loss of brain tissue structure in clinically isolated syndrome. *Mult Scler* 2016;22:1032-9.
 97. Farrell BT, Hamilton BE, Dósa E, Rimely E, Nasser M, Gahramanov S, Lacy CA, Frenkel EP, Doolittle ND, Jacobs PM, Neuwelt EA. Using iron oxide nanoparticles to diagnose CNS inflammatory diseases and PCNSL. *Neurology* 2013;81:256-63.
 98. Kooi ME, Cappendijk VC, Cleutjens KB, Kessels AG, Kitslaar PJ, Borgers M, Frederik PM, Daemen MJ, van Engelsehoven JM. Accumulation of ultrasmall superparamagnetic particles of iron oxide in human atherosclerotic plaques can be detected in vivo magnetic resonance imaging. *Circulation* 2003;107:2453-8.
 99. Trivedi RA, Mallawarachi C, U-King-Im JM, Graves MJ, Horsley J, Goddard MJ, Brown A, Wang L, Kirkpatrick PJ, Brown J, Gillard JH. Identifying inflamed carotid plaques using in vivo USPIO-enhanced MR imaging to label plaque macrophages. *Arterioscler Thromb Vasc Biol* 2006;26:1601-6.
 100. Tang T, Howarth SP, Miller SR, Trivedi R, Graves MJ, King-Im JU, Li ZY, Brown AP, Kirkpatrick PJ, Gaunt ME, Gillard JH. Assessment of inflammatory burden contralateral to the symptomatic carotid stenosis using high resolution ultrasmall, superparamagnetic iron oxide-enhanced MRI. *Stroke* 2006;37:2266-70.
 101. Matijevic N, Wu KK, Howard AG, Wasserman B, Wang WY, Folsom AR, Sharrett AR. Association of blood monocyte and platelet markers with carotid artery characteristics: the Atherosclerosis Risk in Communities Carotid MRI study. *Cerebrovasc Dis* 2011;31:552-8.
 102. Katsargyris A, Tsiodras S, Theocharis S, Giaginis K, Vasileiou I, Bakoyiannis C, Georgopoulos S, Bastounis E, Klonaris C. Toll-like receptor 4 immunohistochemical expression is enhanced in macrophages of symptomatic carotid atherosclerotic plaques. *Cerebrovasc Dis* 2011;31:29-36.
 103. Howarth SP, Tang TY, Trivedi R, Weerakkody R, U-King-Im JM, Gaunt ME, Boyle JR, Li ZY, Miller SR, Graves MJ, Gillard JH. Utility of USPIO-enhanced MR imaging to identify inflammation and the fibrous cap: a comparison of symptomatic and asymptomatic individuals. *Eur J Radiol* 2009;70:555-60.
 104. Degnan AJ, Patterson AJ, Tang TY, Howarth SP, Gillard JH. Evaluation of ultrasmall superparamagnetic iron oxide-enhanced MRI of carotid atherosclerosis to assess risk of cerebrovascular and cardiovascular events: follow-up of the ATHEROMA trial. *Cerebrovasc Dis* 2012;34:169-73.
 105. Yancy AD, Olzinski AR, Hu TC, Lenhard SC, Aravindhan K, Gruver SM, Jacobs PM, Willette RN, Jucker BM. Differential uptake of ferumoxtran-10 and ferumoxytol ultrasmall superparamagnetic iron oxide contrast agents in rabbits: critical determinants of atherosclerotic plaque labeling. *J Magn Reson Imaging* 2005;21:432-42.
 106. Jayaraman T, Berenstein V, Li X, Mayer J, Silane M, Shin YS, Niimi Y, Kiliç T, Gunel M, Berenstein A. Tumor necrosis factor alpha is a key modulator of inflammation in cerebral aneurysms. *Neurosurgery* 2005;57:558-564; discussion 64.
 107. Jayaraman T, Paget A, Shin YS, Li X, Mayer J, Chaudhry H, Niimi Y, Silane M, Berenstein A. TNF-alpha-mediated inflammation in cerebral aneurysms: a potential link to growth and rupture. *Vasc Health Risk Manag* 2008;4:805-17.
 108. Chalouhi N, Ali MS, Jabbour PM, Tjoumakaris SI, Gonzalez LF, Rosenwasser RH, Koch WJ, Dumont AS. Biology of intracranial aneurysms: role of inflammation. *J Cereb Blood Flow Metab* 2012;32:1659-76.
 109. Hasan D, Chalouhi N, Jabbour P, Dumont AS, Kung DK, Magnotta VA, Young WL, Hashimoto T, Winn HR, Heistad D. Early change in ferumoxytol-enhanced magnetic resonance imaging signal suggests unstable human cerebral aneurysm: a pilot study. *Stroke* 2012;43:3258-65.
 110. Hasan DM, Chalouhi N, Jabbour P, Magnotta VA, Kung DK, Young WL. Imaging aspirin effect on macrophages in the wall of human cerebral aneurysms using ferumoxytol-enhanced MRI: preliminary results. *J Neuroradiol* 2013;40:187-91.
 111. Hasan DM, Chalouhi N, Jabbour P, Dumont AS, Kung DK, Magnotta VA, Young WL, Hashimoto T, Richard

- Winn H, Heistad D. Evidence that acetylsalicylic acid attenuates inflammation in the walls of human cerebral aneurysms: preliminary results. *J Am Heart Assoc* 2013;2:e000019.
112. McBride OM, Joshi NV, Robson JM, MacGillivray TJ, Gray CD, Fletcher AM, Dweck MR, van Beek EJ, Rudd JH, Newby DE, Semple SI. Positron Emission Tomography and Magnetic Resonance Imaging of Cellular Inflammation in Patients with Abdominal Aortic Aneurysms. *Eur J Vasc Endovasc Surg* 2016;51:518-26.
113. Jalalzadeh H, Indrakusuma R, Planken RN, Legemate DA, Koelemay MJ, Balm R. Inflammation as a Predictor of Abdominal Aortic Aneurysm Growth and Rupture: A Systematic Review of Imaging Biomarkers. *Eur J Vasc Endovasc Surg* 2016;52:333-42.
114. McBride OM, Berry C, Burns P, Chalmers RT, Doyle B, Forsythe R, Garden OJ, Goodman K, Graham C, Hoskins P, Holdsworth R, MacGillivray TJ, McKillop G, Murray G, Oatey K, Robson JM, Roditi G, Semple S, Stuart W, van Beek EJ, Vesey A, Newby DE. MRI using ultrasmall superparamagnetic particles of iron oxide in patients under surveillance for abdominal aortic aneurysms to predict rupture or surgical repair: MRI for abdominal aortic aneurysms to predict rupture or surgery—the MA(3)RS study. *Open Heart* 2015;2:e000190.
115. Gaglia JL, Harisinghani M, Aganj I, Wojtkiewicz GR, Hedgire S, Benoist C, Mathis D, Weissleder R. Noninvasive mapping of pancreatic inflammation in recent-onset type-1 diabetes patients. *Proc Natl Acad Sci U S A* 2015;112:2139-44.
116. Malosio ML, Esposito A, Brigatti C, Palmisano A, Piemonti L, Nano R, Maffi P, De Cobelli F, Del Maschio A, Secchi A. MR imaging monitoring of iron-labeled pancreatic islets in a small series of patients: islet fate in successful, unsuccessful, and autotransplantation. *Cell Transplant* 2015;24:2285-96.
117. Alam SR, Shah AS, Richards J, Lang NN, Barnes G, Joshi N, MacGillivray T, McKillop G, Mirsadraee S, Payne J, Fox KA, Henriksen P, Newby DE, Semple SI. Ultrasmall superparamagnetic particles of iron oxide in patients with acute myocardial infarction: early clinical experience. *Circ Cardiovasc Imaging* 2012;5:559-65.
118. Yilmaz A, Rösch S, Yildiz H, Klumpp S, Sechtem U. First multiparametric cardiovascular magnetic resonance study using ultrasmall superparamagnetic iron oxide nanoparticles in a patient with acute myocardial infarction: new vistas for the clinical application of ultrasmall superparamagnetic iron oxide. *Circulation* 2012;126:1932-4.
119. Yilmaz A, Dengler MA, van der Kuip H, Yildiz H, Rösch S, Klumpp S, Klingel K, Kandolf R, Helluy X, Hiller KH, Jakob PM, Sechtem U. Imaging of myocardial infarction using ultrasmall superparamagnetic iron oxide nanoparticles: a human study using a multi-parametric cardiovascular magnetic resonance imaging approach. *Eur Heart J* 2013;34:462-75.
120. Richards JM, Shaw CA, Lang NN, Williams MC, Semple SI, MacGillivray TJ, Gray C, Crawford JH, Alam SR, Atkinson AP, Forrest EK, Bienek C, Mills NL, Burdess A, Dhaliwal K, Simpson AJ, Wallace WA, Hill AT, Roddie PH, McKillop G, Connolly TA, Feuerstein GZ, Barclay GR, Turner ML, Newby DE. In vivo mononuclear cell tracking using superparamagnetic particles of iron oxide: feasibility and safety in humans. *Circ Cardiovasc Imaging* 2012;5:509-17.
121. Tanaka M, Nakashima O, Wada Y, Kage M, Kojiro M. Pathomorphological study of Kupffer cells in hepatocellular carcinoma and hyperplastic nodular lesions in the liver. *Hepatology* 1996;24:807-12.
122. Kim YK, Kim CS, Kwak HS, Lee JM. Three-dimensional dynamic liver MR imaging using sensitivity encoding for detection of hepatocellular carcinomas: comparison with superparamagnetic iron oxide-enhanced MR imaging. *J Magn Reson Imaging* 2004;20:826-37.
123. Lee JM, Park JW, Choi BI. 2014 KLCSSG-NCC Korea Practice Guidelines for the management of hepatocellular carcinoma: HCC diagnostic algorithm. *Dig Dis* 2014;32:764-77.
124. Nishie A, Asayama Y, Ishigami K, Tajima T, Kakihara D, Nakayama T, Takayama Y, Okamoto D, Taketomi A, Shirabe K, Fujita N, Obara M, Yoshimitsu K, Honda H. MR prediction of liver fibrosis using a liver-specific contrast agent: Superparamagnetic iron oxide versus Gd-EOB-DTPA. *J Magn Reson Imaging* 2012;36:664-71.
125. Saito K, Yoshimura N, Saguchi T, Park J, Sugimoto K, Akata S, Moriyasu F, Tokuyue K. MR characterization of focal nodular hyperplasia: gadoteric acid versus superparamagnetic iron oxide imaging. *Magn Reson Med* 2012;11:163-9.
126. Bahl G, Cruite I, Wolfson T, Gamst AC, Collins JM, Chavez AD, Barakat F, Hassanein T, Sirlin CB. Noninvasive classification of hepatic fibrosis based on texture parameters from double contrast-enhanced magnetic resonance images. *J Magn Reson Imaging* 2012;36:1154-61.
127. Yokoo T, Wolfson T, Iwaisako K, Peterson MR, Mani

- H, Goodman Z, Changchien C, Middleton MS, Gamst AC, Mazhar SM, Kono Y, Ho SB, Sirlin CB. Evaluation of Liver Fibrosis Using Texture Analysis on Combined-Contrast-Enhanced Magnetic Resonance Images at 3.0T. *Biomed Res Int* 2015;2015:387653.
128. Tanaka Y, Nakazawa T, Inoue T, Yamane K, Kubota K, Uojima H, Takada J, Okuwaki Y, Hidaka H, Shibuya A, Kokubu S, Matsunaga K, Koizumi W. SPIO-enhanced MRI is useful in predicting malignant potential of vascular transformation of hypointense hypovascular nodules on Gd-EOB-DTPA-enhanced MRI. *Hepatol Res* 2016. [Epub ahead of print]. doi: 10.1111/hepr.12850.
 129. Teerasamit W, Saiviroonporn P, Pongpaibul A, Korpraphong P. Benefit of double contrast MRI in diagnosis of hepatocellular carcinoma in patients with chronic liver diseases. *J Med Assoc Thai* 2014;97:540-7.
 130. Maurea S, Mainenti PP, Tambasco A, Imbriaco M, Mollica C, Laccetti E, Camera L, Liuzzi R, Salvatore M. Diagnostic accuracy of MR imaging to identify and characterize focal liver lesions: comparison between gadolinium and superparamagnetic iron oxide contrast media. *Quant Imaging Med Surg* 2014;4:181-9.
 131. Liao J, Shiehorteza M, Girard OM, Sirlin CB, Bydder M. Evaluation of MRI fat fraction in the liver and spine pre and post SPIO infusion. *Magn Reson Imaging* 2013;31:1012-6.
 132. Mikolasevic I, Orlic L, Franjic N, Hauser G, Stimac D, Milic S. Transient elastography (FibroScan®) with controlled attenuation parameter in the assessment of liver steatosis and fibrosis in patients with nonalcoholic fatty liver disease - Where do we stand? *World J Gastroenterol* 2016;22:7236-51.
 133. Allkemper T, Sagmeister F, Cicinnati V, Beckebaum S, Kooijman H, Kanthak C, Stehling C, Heindel W. Evaluation of fibrotic liver disease with whole-liver T1ρ MR imaging: a feasibility study at 1.5 T. *Radiology* 2014;271:408-15.
 134. Koon CM, Zhang X, Chen W, Chu ES, San Lau CB, Wáng YX. Black blood T1rho MR imaging may diagnose early stage liver fibrosis: a proof-of-principle study with rat biliary duct ligation model. *Quant Imaging Med Surg* 2016;6:353-363.
 135. Karlas T, Petroff D, Sasso M, Fan JG, Mi YQ, de Lédighen V, Kumar M, Lupsor-Platon M, Han KH, Cardoso AC, Ferraioli G, Chan WK, Wai-Sun Wong V, Myers RP, Chayama K, Friedrich-Rust M, Beaugrand M, Shen F, Hiriart JB, Sarin SK, Badea R, Sik Jung K, Marcellin P, Filice C, Mahadeva S, Lai-Hung Wong G, Crotty P, Masaki K, Bojunga J, Bedossa P, Keim V, Wiegand J. Individual patient data meta-analysis of controlled attenuation parameter (CAP) technology for assessing steatosis. *J Hepatol* 2016. [Epub ahead of print]. doi: 10.1016/j.jhep.2016.12.022.
 136. Varallyay CG, Nesbit E, Fu R, Gahramanov S, Moloney B, Earl E, Muldoon LL, Li X, Rooney WD, Neuwelt EA. High-resolution steady-state cerebral blood volume maps in patients with central nervous system neoplasms using ferumoxytol, a superparamagnetic iron oxide nanoparticle. *J Cereb Blood Flow Metab* 2013;33:780-6.
 137. Hanneman K, Kino A, Cheng JY, Alley MT, Vasanaawala SS. Assessment of the precision and reproducibility of ventricular volume, function, and mass measurements with ferumoxytol-enhanced 4D flow MRI. *J Magn Reson Imaging* 2016;44:383-92.
 138. Fredrickson J, Serkova NJ, Wyatt SK, Carano RA, Pirzkall A, Rhee I, Rosen LS, Bessudo A, Weekes C, de Crespigny A. Clinical translation of ferumoxytol-based vessel size imaging (VSI): Feasibility in a phase I oncology clinical trial population. *Magn Reson Med* 2017;77:814-25.
 139. Nasserli M, Gahramanov S, Netto JP, Fu R, Muldoon LL, Varallyay C, Hamilton BE, Neuwelt EA. Evaluation of pseudoprogession in patients with glioblastoma multiforme using dynamic magnetic resonance imaging with ferumoxytol calls RANO criteria into question. *Neuro Oncol* 2014;16:1146-54.
 140. Gahramanov S, Muldoon LL, Varallyay CG, Li X, Kraemer DF, Fu R, Hamilton BE, Rooney WD, Neuwelt EA. Pseudoprogession of glioblastoma after chemo- and radiation therapy: diagnosis by using dynamic susceptibility-weighted contrast-enhanced perfusion MR imaging with ferumoxytol versus gadoteridol and correlation with survival. *Radiology* 2013;266:842-52.
 141. Netto JP, Schwartz D, Varallyay C, Fu R, Hamilton B, Neuwelt EA. Misleading early blood volume changes obtained using ferumoxytol-based magnetic resonance imaging perfusion in high grade glial neoplasms treated with bevacizumab. *Fluids Barriers CNS* 2016;13:23.
 142. Qiu D, Zaharchuk G, Christen T, Ni WW, Moseley ME. Contrast-enhanced functional blood volume imaging (CE-fBVI): enhanced sensitivity for brain activation in humans using the ultrasmall superparamagnetic iron oxide agent ferumoxytol. *Neuroimage* 2012;62:1726-31.
 143. Mandeville JB. IRON fMRI measurements of CBV and implications for BOLD signal. *Neuroimage* 2012;62:1000-8.
 144. Baumgartner R, Cho W, Coimbra A, Chen C, Wang Z,

- Struyk A, Venketasubramanian N, Low M, Gargano C, Zhao F, Williams D, Reese T, Seah S, Feng D, Apreleva S, Petersen E, Evelhoch JL. Evaluation of an fMRI USPIO-based assay in healthy human volunteers. *J Magn Reson Imaging* 2016. [Epub ahead of print]. doi: 10.1002/jmri.25499.
145. D'Arceuil H, Coimbra A, Triano P, Dougherty M, Mello J, Moseley M, Glover G, Lansberg M, Blankenberg F. Ferumoxytol enhanced resting state fMRI and relative cerebral blood volume mapping in normal human brain. *Neuroimage* 2013;83:200-9.
 146. Florian A, Ludwig A, Rösch S, Yildiz H, Klumpp S, Sechtem U, Yilmaz A. Positive effect of intravenous iron-oxide administration on left ventricular remodelling in patients with acute ST-elevation myocardial infarction - a cardiovascular magnetic resonance (CMR) study. *Int J Cardiol* 2014;173:184-9.
 147. Smits LP, Coolen BF, Panno MD, Runge JH, Nijhof WH, Verheij J, Nieuwdorp M, Stoker J, Beuers UH, Nederveen AJ, Stroes ES. Noninvasive Differentiation between Hepatic Steatosis and Steatohepatitis with MR Imaging Enhanced with USPIOs in Patients with Nonalcoholic Fatty Liver Disease: A Proof-of-Concept Study. *Radiology* 2016;278:782-91.
 148. Gleich B, Weizenecker J. Tomographic imaging using the nonlinear response of magnetic particles. *Nature* 2005;435:1214-7.
 149. Konkle JJ, Goodwill PW, Carrasco-Zevallos OM, Conolly SM. Projection reconstruction magnetic particle imaging. *IEEE Trans Med Imaging* 2013;32:338-47.
 150. Haegele J, Rahmer J, Gleich B, Borgert J, Wojtczyk H, Panagiotopoulos N, Buzug TM, Barkhausen J, Vogt FM. Magnetic particle imaging: visualization of instruments for cardiovascular intervention. *Radiology* 2012;265:933-8.
 151. Haegele J, Panagiotopoulos N, Cremers S, Rahmer JR, Franke J, Duschka RL, Vaalma S, Heidenreich M, Borgert JR, Borm P, Barkhausen JR, Vogt FM. Magnetic Particle Imaging: A Resovist Based Marking Technology for Guide Wires and Catheters for Vascular Interventions. *IEEE Trans Med Imaging* 2016;35:2312-8.
 152. Haegele J, Vaalma S, Panagiotopoulos N, Barkhausen J, Vogt FM, Borgert J, Rahmer J. Multi-color magnetic particle imaging for cardiovascular interventions. *Phys Med Biol* 2016;61:N415-26.
 153. Kakite S, Fujii S, Nakamatsu S, Kanasaki Y, Yamashita E, Matsusue E, Ouchi Y, Kaminou T, Tokunaga S, Koda M, Ogawa T. Usefulness of administration of SPIO prior to RF ablation for evaluation of the therapeutic effect: an experimental study using miniature pigs. *Eur J Radiol* 2011;78:282-6.
 154. Cheng KK, Chan PS, Fan S, Kwan SM, Yeung KL, Wang YX, Chow AH, Wu EX, Baum L. Curcumin-conjugated magnetic nanoparticles for detecting amyloid plaques in Alzheimer's disease mice using magnetic resonance imaging (MRI). *Biomaterials* 2015;44:155-72.
 155. Haacke EM, Xu Y, Cheng YC, Reichenbach JR. Susceptibility weighted imaging (SWI). *Magn Reson Med* 2004;52:612-8.
 156. Sehgal V, Delproposto Z, Haacke EM, Tong KA, Wycliffe N, Kido DK, Xu Y, Neelavalli J, Haddar D, Reichenbach JR. Clinical applications of neuroimaging with susceptibility-weighted imaging. *J Magn Reson Imaging* 2005;22:439-50.
 157. Acosta-Cabronero J, Williams GB, Cardenas-Blanco A, Arnold RJ, Lupson V, Nestor PJ. In vivo quantitative susceptibility mapping (QSM) in Alzheimer's disease. *PLoS One* 2013;8:e81093.
 158. Patil R, Gangalum PR, Wagner S, Portilla-Arias J, Ding H, Rekechenetskiy A, Konda B, Inoue S, Black KL, Ljubimova JY, Holler E. Curcumin Targeted, Polymalic Acid-Based MRI Contrast Agent for the Detection of A β Plaques in Alzheimer's Disease. *Macromol Biosci* 2015;15:1212-7.
 159. Ohno K, Akashi T, Tsujii Y, Yamamoto M, Tabata Y. Blood clearance and biodistribution of polymer brush-afforded silica particles prepared by surface-initiated living radical polymerization. *Biomacromolecules* 2012;13:927-36.
 160. Ohno K, Mori C, Akashi T, Yoshida S, Tago Y, Tsujii Y, Tabata Y. Fabrication of contrast agents for magnetic resonance imaging from polymer-brush-afforded iron oxide magnetic nanoparticles prepared by surface-initiated living radical polymerization. *Biomacromolecules* 2013;14:3453-62.
 161. Chen T, Mori Y, Inui-Yamamoto C, Komai Y, Tago Y, Yoshida S, Takabatake Y, Isaka Y, Ohno K, Yoshioka Y. Polymer-brush-afforded SPIO Nanoparticles Show a Unique Biodistribution and MR Imaging Contrast in Mouse Organs. *Magn Reson Med Sci* 2017. [Epub ahead of print]. doi: 10.2463/mrms.mp.2016-0067.
 162. Cukur T, Yamada M, Overall WR, Yang P, Nishimura DG. Positive contrast with alternating repetition time SSFP (PARTS): a fast imaging technique for SPIO-labeled cells. *Magn Reson Med* 2010;63:427-37.
 163. Chen W. Artifacts correction for T1rho imaging with constant amplitude spin-lock. *J Magn Reson* 2017;274:13-23.

164. Chen W. Errors in quantitative T1rho imaging and the correction methods. *Quant Imaging Med Surg* 2015;5:583-91.
165. Stuber M, Gilson WD, Schär M, Kedziorek DA, Hofmann LV, Shah S, Vonken EJ, Bulte JW, Kraitchman DL. Positive contrast visualization of iron oxide-labeled stem cells using inversion-recovery with ON-resonant water suppression (IRON). *Magn Reson Med* 2007;58:1072-7.
166. Pelot NA, Bowen CV. Quantification of superparamagnetic iron oxide using inversion recovery balanced steady-state free precession. *Magn Reson Imaging* 2013;31:953-60.
167. Wang L, Corum CA, Idiyatullin D, Garwood M, Zhao Q. T1 estimation for aqueous iron oxide nanoparticle suspensions using a variable flip angle SWIFT sequence. *Magn Reson Med* 2013;70:341-7.
168. Moonen RP, van der Tol P, Hectors SJ, Starmans LW, Nicolay K, Strijkers GJ. Spin-lock MR enhances the detection sensitivity of superparamagnetic iron oxide particles. *Magn Reson Med* 2015;74:1740-9.

Cite this article as: Wáng YX, Idée JM. A comprehensive literatures update of clinical researches of superparamagnetic resonance iron oxide nanoparticles for magnetic resonance imaging. *Quant Imaging Med Surg* 2017;7(1):88-122. doi: 10.21037/qims.2017.02.09